

# Field-theoretical study of the Bose polaron

Steffen Patrick Rath<sup>1</sup> and Richard Schmidt<sup>1,2,3</sup>

<sup>1</sup>*Technische Universität München, James-Frank-Straße, 85748 Garching, Germany*

<sup>2</sup>*Department of Physics, Harvard University, Cambridge, MA 02138, USA*

<sup>3</sup>*ITAMP, Harvard-Smithsonian Center for Astrophysics, Cambridge, MA 02138, USA*

(Dated: December 17, 2013)

We study the properties of the Bose polaron, an impurity strongly interacting with a Bose–Einstein condensate, using a field-theoretic approach and make predictions for the spectral function and various quasiparticle properties that can be tested in experiment. We find that most of the spectral weight is contained in a coherent attractive and a metastable repulsive polaron branch. We show that the qualitative behavior of the Bose polaron is well described by a non-selfconsistent T-matrix approximation by comparing analytical results to numerical data obtained from a fully selfconsistent T-matrix approach. The latter takes into account an infinite number of bosons excited from the condensate.

PACS numbers: 67.85.-d, 67.85.Pq, 67.90.+z

## I. INTRODUCTION

Quantum impurity problems are among the paradigms of quantum many-body physics. While they provide one of the conceptually simplest ways to probe their host medium [1], they are also of interest in their own right. A classic example is the Landau–Pekar polaron [2, 3], a single charge moving inside a polarizable medium. While hardly deforming the medium itself, the impurity tends to self-localize for sufficiently strong interactions. Fröhlich derived an effective Hamiltonian for this particular system [4] which since has found much application also for microscopically different systems. Girardeau was the first to study a neutral impurity immersed in superfluid <sup>4</sup>He [5]. With the advent of cold atoms, which in recent years have proven a versatile testbed for the study of quantum many-body systems [6], new possibilities for the study of quantum impurities have emerged. The host may consist of bosons or fermions, interactions are tunable via Feshbach resonances and even the dimensionality of the system can be engineered [7]. The case of the Fermi polaron where the host medium is an ideal Fermi gas has received considerable experimental attention. In particular, the technique of inverse radiofrequency (rf) spectroscopy has permitted the study of the Fermi polaron’s spectral function both in two and three dimensions [7–9].

The Bose polaron problem, where an impurity interacts with a Bose–Einstein condensate (BEC), has so far not been studied very extensively in experiment, with the existing literature mostly focusing on weakly interacting systems [10–13]. With the recent progress on the identification and characterization of Feshbach resonances in ultracold Bose-Fermi mixtures [14–17], experiments with impurities featuring widely tunable interactions with a BEC now seem within reach. In step with experimental technology, most of the theoretical literature on the Bose polaron has focused on weak interspecies interactions. Two particularly well studied approaches are on the one hand coupled mean field equations which permit the characterization of polaron self-localization [18–23],

and on the other hand the study of an effective Fröhlich-type Hamiltonian [24–29] which has also been applied to the description of Bose–Fermi mixtures [30–35].

In contrast to these effective approaches which rely on the microscopic repulsion between the impurity and the host atoms, we start from a microscopic description of the impurity interacting with a homogeneous BEC via a Feshbach resonance which takes into account the attractiveness of the interactions. Analyzing the excitation spectrum, we find two branches. While the first is a stable, long-lived quasiparticle representing an attractive polaron, the second can be interpreted as a repulsive polaron. The finite lifetime of the latter is a consequence of the attractive interactions and it inhibits the preparation of the system in a stable strongly repulsive state, thus complicating a quantum simulation of the Landau–Pekar polaron paradigm. To circumvent the possibility of an instability towards a ground state with an inhomogeneous BEC, we consider a setup where the impurity is driven from a weakly interacting initial state to a final state strongly interacting with a homogeneous condensate. We provide predictions for the momentum-resolved spectral function which can be experimentally tested with available technology [7, 9, 36–38]. Within a T-matrix approach, we find that to a surprisingly good approximation, the selfenergy of the Bose polaron is proportional to the bare interspecies T-matrix. We show that the leading correction arises not due to weak boson–boson interactions, but due to a selfconsistent treatment of the interaction of the impurity with the BEC which takes into account multiple virtual excitations of bosons out of the condensate.

## II. THE MODEL

We consider a mobile impurity of mass  $m_\psi$  which is immersed in a Bose–Einstein condensate (BEC) of atoms of mass  $m_\phi$  and density  $n$  at temperature  $T = 0$ . Although in the case of a single impurity its statistics is of no con-

sequence, we will nonetheless refer to it as a fermion, having in mind the Bose polaron problem as a Bose-Fermi mixture in the limit of extreme population imbalance  $n_\psi/n \ll 1$  [92]. We assume that the bosons interact weakly among each other while they interact with the impurity via a, potentially strong, short-range potential as appropriate for ultracold atoms close to a magnetically tunable Feshbach resonance [39]. In the case of an open-channel dominated Feshbach resonance (a description appropriate for Feshbach resonances of arbitrary width is discussed in Appendix A), the system can be described using a contact interaction [6] and the corresponding microscopic, euclidean action reads (throughout the paper, we use units in which  $\hbar = 1$ )

$$S = \int d\tau \int d^3x \left\{ \varphi_{\mathbf{x},\tau}^* \left( \partial_\tau - \frac{1}{2m_\phi} \nabla^2 - \mu_\phi \right) \varphi_{\mathbf{x},\tau} + \psi_{\mathbf{x},\tau}^* \left( \partial_\tau - \frac{1}{2m_\psi} \nabla^2 - \mu_\psi \right) \psi_{\mathbf{x},\tau} + \frac{g_{\phi\phi}}{2} |\varphi_{\mathbf{x},\tau}|^4 + \tilde{g}_{\phi\psi} |\varphi_{\mathbf{x},\tau}|^2 |\psi_{\mathbf{x},\tau}|^2 \right\}, \quad (1)$$

where  $\varphi$  denotes the bosonic,  $\psi$  the impurity field, and  $\mu_\phi$  and  $\mu_\psi$  the corresponding chemical potentials. The mi-

croscopic couplings  $g_{\phi\phi}$  and  $\tilde{g}_{\phi\psi}$  are related to the experimentally relevant scattering lengths  $a_{\phi\phi}$  and  $a_{\phi\psi}$  via the solution of the two-body Lippmann-Schwinger equation. While the resulting relation between  $g_{\phi\phi}$  and  $a_{\phi\phi}$  is trivial due to the weakness of the boson-boson coupling and gives rise to the common identity  $g_{\phi\phi} \approx 4\pi a_{\phi\phi}/m_\phi > 0$ , it is more complicated in the case of the interspecies coupling where the scattering length may become arbitrarily large (cf. Appendix B). In Eq. (1) we allow for an arbitrary mass imbalance  $\alpha = m_\psi/m_\phi$ . While for our numerical results we assume the mass-balanced case, we show all analytical results for the general case where  $\alpha \neq 1$ .

In the following, we use an effective action which is based on the Bogoliubov approximation and may be obtained as follows. In a first step, we exploit the shift symmetry of the path integral and make the usual replacement  $\varphi(\mathbf{x}, t) \mapsto \sqrt{\rho_0(\mathbf{x})} + \phi(\mathbf{x}, t)$  where  $\rho_0(\mathbf{x}) > 0$  is the condensate density and  $\phi(\mathbf{x}, t)$  represents the fluctuations around the condensate. We expand around a homogeneous condensate and make the simplifying assumption that the condensate density is not altered by the presence of the impurity, i.e., we replace the condensate by its mean field value  $\rho_0(\mathbf{x}) \equiv \rho_0 = n$ . Following Bogoliubov's prescription, we discard all powers of the bosonic fields higher than two. After some rearrangements, the resulting effective action can be written as

$$S_{\text{eff}} = \int_p \left\{ \frac{1}{2} \begin{pmatrix} \phi_p^* \\ \phi_{-p} \end{pmatrix} \begin{pmatrix} -[G_\phi^{(0)}(-p)]^{-1} & g_{\phi\phi}\rho_0 \\ g_{\phi\phi}\rho_0 & -[G_\phi^{(0)}(p)]^{-1} \end{pmatrix} \begin{pmatrix} \phi_p \\ \phi_{-p}^* \end{pmatrix} + \psi_p^* \left( -i\omega + \frac{\mathbf{p}^2}{2m_\psi} - \mu_\psi \right) \psi_p \right\} + \tilde{g}_{\phi\psi} \int_x |\psi_x|^2 [|\phi_x|^2 + (\phi_x + \phi_x^*)\sqrt{\rho_0} + \rho_0] \quad (2)$$

where we have introduced the shorthand notation  $p = (\omega, \mathbf{p})$  and  $x = (\tau, \mathbf{x})$ .  $[G_\phi^{(0)}(p)]^{-1} = i\omega - \mathbf{p}^2/2m_\phi + g_{\phi\phi}\rho_0$  is the inverse bare bosonic propagator. The chemical potential  $\mu_\phi = g_{\phi\phi}\rho_0$  follows from the Hugenholtz-Pines relation [40] evaluated at the mean field level and vanishes in the case of a non-interacting BEC. The bosonic propagator is obtained by inverting the matrix appearing in Eq. (2). Only two of the four matrix elements are independent, namely the normal and the anomalous propagator which are given by [41]

$$G_{11}^\phi(i\omega, \mathbf{p}) = -\frac{i\omega + \frac{\mathbf{p}^2}{2m_\phi} + g_{\phi\phi}\rho_0}{\omega^2 + \varepsilon_p^2} \xrightarrow{g_{\phi\phi} \rightarrow 0} G_\phi^{(0)}(i\omega, \mathbf{p}) \quad (3)$$

$$G_{21}^\phi(i\omega, \mathbf{p}) = \frac{g_{\phi\phi}\rho_0}{\omega^2 + \varepsilon_p^2} \xrightarrow{g_{\phi\phi} \rightarrow 0} 0 \quad (4)$$

with the Bogoliubov dispersion

$$\varepsilon_p = \sqrt{\frac{\mathbf{p}^2}{2m_\phi} \left( \frac{\mathbf{p}^2}{2m_\phi} + 2g_{\phi\phi}\rho_0 \right)} \xrightarrow{g_{\phi\phi} \rightarrow 0} \frac{\mathbf{p}^2}{2m_\phi}. \quad (5)$$

In Eqs. (3)-(5) we indicate the limit of the non-interacting Bose gas which we will study below as a limiting case of our model. The bare impurity propagator in Eq. (2) has the usual form

$$G_\psi^{(0)}(i\omega, \mathbf{p}) = \frac{1}{i\omega - \frac{\mathbf{p}^2}{2m_\psi} + \mu_\psi}. \quad (6)$$

By using the effective action (2) with a homogeneous BEC we neglect that for strong enough interspecies interactions, the actual mean field solution corresponding to the action (1) may feature an inhomogeneous condensate [93]. In fact, self-localization of the impurity and deformations of the BEC have been predicted

for both microscopically repulsive and attractive interactions [19, 21–23, 42] as well as in the context of a two-fluid Bose–Bose mixture [43]. Our neglecting these effects in the study of the model (2) can be justified by considering the involved time scales. The deformation of the BEC requires the displacement of mass which in weakly interacting BECs typically happens on a time scale of  $\tau_{\text{BEC}} \sim \hbar/(g_{\phi\phi}n)$  [23]. In this article we are, however, interested in the excitation spectrum of the Bose polaron which can be experimentally probed via inverse radio frequency spectroscopy. Here the impurity atom is driven from a weakly to a strongly interacting state. In such experiments the time scale is set by a small fraction of the inverse Rabi frequency, which can be significantly smaller than  $\tau_{\text{BEC}}$  [9]. In consequence, the rf response of the system is determined by the spectral function of an impurity interacting with a homogeneous condensate and our model is expected to apply even in the strongly interacting regime.

### III. NON-SELFCONSISTENT T-MATRIX APPROXIMATION

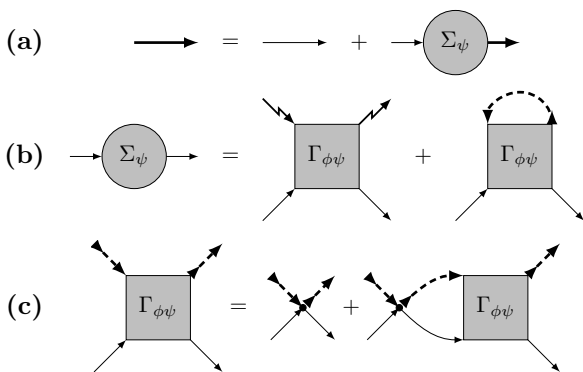


FIG. 1: Diagrams corresponding to the non-selfconsistent T-matrix approximation: (a) Dyson’s equation for the impurity Green’s function. (b) Impurity selfenergy. (c) In-medium T-matrix equation. Solid thin lines stand for impurity propagators while dashed lines represent normal Bose propagators. The zig-zag lines denote in- and outgoing condensate particles. In the case of the selfconsistent T-matrix approximation discussed in Section IV, the solid thin line (bare fermion propagator) in the particle–particle loop in (c) is replaced by the thick line from (a) representing the dressed fermion propagator.

The derivation of the NSCT equations is based on the perturbative expansion of the impurity Green’s function in the bare coupling constant  $\tilde{g}_{\phi\psi}$ . Using Dyson’s equation [cf. Fig. 1 (a)], one automatically resums all one-particle reducible Feynman diagrams into the self-energy  $\Sigma_\psi$ . Taking into account the diagrams shown in

Fig. 1 (b), the latter reads

$$\Sigma_\psi(\Omega, \mathbf{p}) = \rho_0 \Gamma_{\phi\psi}(\Omega, \mathbf{p}) - \int_{\mathbf{k}} \int_{\nu} G_{11}^\phi[i(\nu - \omega), \mathbf{k} - \mathbf{p}] \Gamma_{\phi\psi}(i\nu, \mathbf{k}) \Big|_{i\omega \rightarrow \Omega + i0^+} \quad (7)$$

where  $\int_{\mathbf{k}} = \int d^3k/(2\pi)^3$ ,  $\int_{\nu} = \int d\nu/2\pi$  and  $\Gamma_{\phi\psi}$  is the in-medium T-matrix. The first term corresponds to the Belyaev-type diagram in Fig. 1 (b) ([44], cf. [45, 46] for recent work on dilute Bose gases building on Belyaev’s technique) and represents a mean field like interaction of the impurity with the condensate. In the case of a Bose gas in the normal phase, this term is absent. The second term reflects the dressing of the impurity with bosons which are depleted from the condensate due to the boson–boson interactions and vanishes in the case of a noninteracting Bose gas. In a calculation at  $T \neq 0$  this term would equally account for scattering off thermally depleted particles. Within the NSCT approximation, the selfenergy only contains the class of two-particle reducible ladder-type diagrams shown in Fig. 1 (c). The T-matrix  $\Gamma_{\phi\psi}$  is given by the infinite sum over this class of diagrams which represents the repeated boson–impurity scattering in the *s*-wave particle–particle channel,

$$\Gamma_{\phi\psi}(\Omega, \mathbf{p}) = \left[ g_{\phi\psi}^{-1} + L(\Omega, \mathbf{p}) \right]^{-1} \quad (8)$$

with the pair propagator

$$L(\Omega, \mathbf{p}) = \int_{\mathbf{k}} \left\{ \int_{\nu} G_{11}^\phi(i\nu, \mathbf{k}) G_\psi^{(0)}[i(\omega - \nu), \mathbf{p} - \mathbf{k}] - \frac{2\alpha m_\phi}{(\alpha + 1)\mathbf{k}^2} \right\} \Big|_{i\omega \rightarrow \Omega + i0^+} \quad (9)$$

We note that in the integral both free particle and Bogoliubov dispersions appear. This reflects the possible scattering of the impurity off phonons with linear dispersion at low scattering energies while at large energies it effectively scatters off the “fundamental” bosons. While the imaginary frequencies used so far provide a particularly clear way of evaluating frequency integrals, we ultimately want to compare with experimentally observable dynamical properties such as rf spectra and quasiparticle properties. To this end, we will consider all quantities at real frequencies obtained by analytic continuation  $i\omega \mapsto \omega + i0^+$  which yields the retarded Green’s function. As a convenient shorthand notation we introduce  $\Omega = \omega + \mu_\psi$  as already used in Eqs. (7) and (9).

The term in the second line of Eq. (9) originates from the renormalization of the bare coupling  $\tilde{g}_{\phi\psi}$ . As discussed in detail in Appendix B, the particle–particle loop has an ultraviolet divergence which is regularized at a momentum cutoff scale  $\Lambda$ . The dependence on  $\Lambda$  is subsequently absorbed in the definition of the bare coupling constant  $\tilde{g}_{\phi\psi}$ , yielding the renormalized interspecies coupling constant

$$g_{\phi\psi}^{-1} = \tilde{g}_{\phi\psi}^{-1} + \int \frac{d^3k}{(2\pi)^3} \frac{2\alpha m_\phi}{(\alpha + 1)\mathbf{k}^2} = \frac{\alpha m_\phi}{2\pi(\alpha + 1)} a_{\phi\psi}^{-1}, \quad (10)$$

where  $\alpha m_\phi/(\alpha + 1)$  is the reduced mass for boson–impurity collisions.

The NSCT approximation has first been used to describe rf experiments on imbalanced Fermi gases and the Fermi polaron (e.g., [47–50]). In the case of two-component fermions it is equivalent to a leading order  $1/N$  expansion [51] and the Nozières–Schmitt-Rink approach [52]. In the context of the Fermi polaron problem (where it turns out to be equivalent to a calculation using a variational wave function [53]), the NSCT approximation has successfully been applied [48] and yields results for various quasiparticle properties in quantitative agreement with experiments [9, 37] and state of the art diagrammatic Monte-Carlo methods [54, 55]. Finally we mention that the NSCT approximation has been employed by Fratini and coworkers [56] for the study of the phase diagram of the Bose–Fermi action (1) in the case of a finite boson and fermion density. In this study the bosons were, however, in the non-condensed phase. Note that the ladder diagrams from Fig. 1 (c) incorporate the dominant pairing fluctuations present in the system. Their resummation is essential to obtain the attractive and repulsive polaron features mentioned in the introduction. These pairing fluctuations are taken into account neither in a diagrammatic expansion based on the Fröhlich Hamiltonian [24, 30, 32–35] nor in mean field approaches [18–23].

In the case of the Bose polaron, there are two particularities compared to the case of two-component fermions or a Bose-Fermi mixture in the normal phase. First, the dashed lines appearing in the loop expressions in Fig. 1 represent not simple bare boson propagators but the mean field Green’s functions including the condensate and featuring a double-pole structure with Bogoliubov dispersion, cf. Eqs. (3) and (5). Second, the presence of the condensate leads to the appearance of additional diagrams where the in- and outgoing lines of the T-matrix represent atoms ejected out of or injected into the condensate [94]. Note that within the T-matrix approximation, the term  $\tilde{g}_{\phi\psi}\rho_0$ —as also implied by the notation for the effective action (2)—is included in the interaction part of the action instead of being incorporated in the bare Fermi propagator or absorbed in the chemical potential. These latter choices would lead to inconsistent expressions involving both renormalized and unrenormalized couplings.

Of course, the T-matrix approach is a non-perturbative approximation. In this respect, beyond the second term in the self-energy in Fig.-1(b), there are more processes which contribute and which we do not take into account. In fact, the diagrammatic structure of our T-matrix approximation is basically the same as in the description of a BEC within a T-matrix approximation with respect to the boson–boson coupling (cf. [45] and references therein). For instance, like in the purely bosonic case, we ignore diagrams in the selfenergy featuring anomalous Bose propagators or vertex corrections. These processes cannot be included in the T-matrix approximation

scheme without causing inconsistencies such as double counting. The T-matrix approach however correctly includes the pairing correlations responsible for the leading instability in the case of ultracold atoms close to a Feshbach resonance. Thus, it allows to access the strong-coupling regime and to reveal the intricate physics beyond the Fröhlich polaron paradigm. Note that also in the case of a weak boson–boson interaction the pairing channel remains dominant. Processes featuring, for instance, anomalous propagators represent only corrections. This is particularly apparent as the anomalous propagator scales with  $g_{\phi\phi}$  while the pairing instability survives the limit  $g_{\phi\phi} \rightarrow 0$ . We thus expect the T-matrix approximation to be a valid description of the Bose polaron in the regime where the host is a weakly interacting Bose gas.

Remarkably, the pair propagator  $L(\Omega, \mathbf{p})$  can be determined fully analytically for arbitrary frequencies, momenta, mass ratios and interaction constants. This is an important feature also for the numerical calculation of spectral functions as it reduces the numerical effort by orders of magnitude and allows for a direct analytical continuation of the results to real frequencies. Since the derivation is somewhat lengthy, we refer to Appendix C for the detailed calculation. However, to illustrate the general structure of the solution, we show here the particularly simple result one obtains in the special case  $\alpha = 1$  and  $p = 0$  where the real and imaginary part of the pair propagator read

$$\text{Re}L(\Omega) = \frac{-1}{2\pi^2} \begin{cases} \sqrt{g_{\phi\phi}} - \frac{\arctan \sqrt{-1 - \frac{\Omega}{g_{\phi\phi}}}}{\sqrt{-g_{\phi\phi} - \Omega}} \Omega & \Omega < -1 \\ \sqrt{g_{\phi\phi}} - \frac{\text{atanh} \sqrt{1 + \frac{\Omega}{g_{\phi\phi}}}}{\sqrt{g_{\phi\phi} + \Omega}} \Omega & -1 \leq \Omega \leq 0 \\ \sqrt{g_{\phi\phi}} - \frac{\text{atanh} \frac{1}{\sqrt{1 + \frac{\Omega}{g_{\phi\phi}}}}}{\sqrt{g_{\phi\phi} + \Omega}} \Omega & 0 < \Omega \end{cases} \quad (11)$$

and

$$\text{Im}L(\Omega, 0) = \frac{1}{4\pi} \frac{\Omega}{\sqrt{g_{\phi\phi} + \Omega}} \theta(\Omega). \quad (12)$$

In these equations as well as the remainder of this article, we adopt units in which  $m_\phi = n = 1$ , i.e., the length scale is set by the mean interparticle spacing  $\sim n^{-1/3}$  of the bosons. Occasionally we will retain the explicit  $m_\phi$  and  $n$  (or  $\rho_0$ ) dependence for clarity. In Fig. 10 in Appendix C, we plot the pair propagator as a function of frequency and momentum (note that for calculational convenience this Appendix uses a different set of units). In the limit  $g_{\phi\phi} \rightarrow 0$  the pair propagator—now again for arbitrary mass ratio—reduces to

$$L(\Omega, \mathbf{p}) = \frac{i}{4\pi} \left( \frac{2\alpha}{\alpha + 1} \right)^{3/2} \sqrt{\Omega - \frac{\mathbf{p}^2}{2(\alpha + 1)} + i0^+}. \quad (13)$$

The corresponding T-matrix obtained via Eq. (8) is identical to the T-matrix in vacuum up to the appearance of the chemical potential  $\mu_\psi$  inside  $\Omega$ .

Having obtained the T-matrix  $\Gamma_{\phi\psi}$  explicitly, we next turn to the calculation of the corresponding impurity self-energy. The frequency integral in Eq. (7) can be performed analytically since the vanishing impurity density dictates that the T-matrix has all its singularities in the lower half plane when one uses imaginary frequencies. The integration contour may thus be closed in the upper half plane and the integral picks up a contribution from one of the boson propagator's poles. After analytic continuation, the selfenergy (7) then reads

$$\begin{aligned} \Sigma_{\psi}(\Omega, \mathbf{p}) &= \Gamma_{\phi\psi}(\Omega, \mathbf{p}) \\ &- \int \frac{d^3k}{(2\pi)^3} \frac{\sqrt{k^2(k^2 + 4g_{\phi\phi})} - (k^2 + 2g_{\phi\phi})}{2\sqrt{k^2(k^2 + 4g_{\phi\phi})}} \\ &\times \Gamma_{\phi\psi} \left( \Omega - \frac{1}{2}\sqrt{k^2(k^2 + 4g_{\phi\phi})}, \mathbf{k} + \mathbf{p} \right). \end{aligned} \quad (14)$$

The remaining momentum integral is readily evaluated numerically.

The main focus of this article is on the excitation spectrum of the impurity. The key theoretical quantity to extract this spectrum is the spectral function of the polaron given by

$$A_{\text{pol}}(\Omega, \mathbf{p}) = -2 \text{Im} G_{\psi}^{\text{R}}(\Omega, \mathbf{p}) \quad (15)$$

with the full retarded impurity Green's function

$$G_{\psi}^{\text{R}}(\Omega, \mathbf{p}) = \frac{1}{\Omega - \frac{\mathbf{p}^2}{2m_{\psi}} - \Sigma_{\psi}(\Omega, \mathbf{p}) + i0^+} \quad (16)$$

as obtained from Dyson's equation depicted in Fig. 1 (a). We will suppress the superscript R in the following and the retardedness of propagators will be implied by the use of the real frequency argument  $\Omega \equiv \omega + \mu_{\psi}$ . Using our conventions, the spectral function fulfills the sum rule  $(2\pi)^{-1} \int d\Omega A_{\text{pol}}(\Omega, \mathbf{p}) = 1$  where the integration extends over all frequencies.

The excitation spectrum contained in the impurity spectral function Eq. (15) is determined by the analytical structure of the Green's function Eq. (16) in the complex frequency plane. While branch cuts correspond to an incoherent continuum of excitations, poles are linked to the existence of well-defined quasiparticles that can be characterized by a small set of key quantities [41]: (i) The quasiparticle dispersion relation  $E(p)$  is defined as the solution of

$$E(p) - \frac{p^2}{2m_{\psi}} - \text{Re}\Sigma_{\psi}[E(p), p] = 0, \quad (17)$$

where in the isotropic case considered here quantities depend only on the magnitude of the momentum  $p = |\mathbf{p}|$  (From here on the symbol  $p$  denotes the magnitude of momentum and not the four-momentum). (ii) The (momentum dependent) spectral weight is given by

$$Z(p) = \frac{1}{1 - \partial_{\Omega} \text{Re}\Sigma_{\psi}[\Omega, p]} \Big|_{\Omega=E(p)}. \quad (18)$$

(iii) The decay width is obtained from

$$\gamma(p) = -Z(p) \text{Im}\Sigma_{\psi}[E(p), p] \quad (19)$$

and (iv) the momentum dependent effective mass reads

$$m^*(p) = \frac{p}{\partial_p E(p)} = \frac{1/Z(p)}{\frac{1}{\alpha} + \frac{1}{p} \partial_p \text{Re}\Sigma_{\psi}[\Omega, p] \Big|_{E(p)}}. \quad (20)$$

Eqs. (17)–(20) provide an accurate description of the quasiparticle properties as long as the poles of the Green's function  $G_{\psi}(\Omega, p)$  in the complex frequency plane are close to the real axis. If this condition is violated, the interpretation of the poles as well-defined quasiparticles starts to break down and the preciseness of Eqs. (17)–(20) depends on how well one satisfies the assumption that  $\text{Im}\Sigma_{\psi}$  remains constant across the width of the quasiparticle peak as well as the smallness of the decay width compared to the quasiparticle energy.

We now turn to the analysis of the impurity's spectral function  $A_{\text{pol}}$  given by Eqs. (15), (16), and (14). When choosing  $\alpha = 1$ , as done for all plots in this article, we are left with  $A_{\text{pol}}$  as a function of four quantities:  $\Omega$ ,  $p$ ,  $a_{\phi\psi}$  and  $a_{\phi\phi}$ . We choose  $n^{1/3}a_{\phi\phi} = 0.1$  for the following plots which is actually about one order of magnitude stronger than what is typical for weakly interacting Bose gases. While such strong interactions have actually been reached in experiment [57–60] and do themselves lead to interesting physics beyond the scope of this article, our motivation for this large value is quite mundane: it turns out that in the T-matrix approximation the dependence of the spectral properties on  $g_{\phi\phi}$  is very weak. So, to make this dependence clearly visible in our plots, we choose this somewhat exaggerated value.

In Fig. 2 we show the impurity spectral function calculated using the NSCT approximation and evaluated at vanishing momentum as a function of the dimensionless quantities  $\Omega/\Omega_0$  and  $(n^{1/3}a_{\phi\psi})^{-1}$ , where  $\Omega_0 = n^{2/3}/m_{\phi}$ . The spectral function shows a continuous background for positive frequencies  $\Omega$  carrying little spectral weight and is dominated by two sharply peaked features, one at positive and one at negative  $\Omega$ . The sharp feature appearing at low energies can be interpreted as an attractive polaron. It is a sharp quasiparticle excitation giving rise to a delta peak in the spectral function which carries most of the spectral weight for large negative values of  $a_{\phi\psi}^{-1}$ . In this weak coupling regime we recover the perturbative result for the polaron's energy which asymptotically obeys  $E_{\text{att}} \sim g_{\phi\psi}n$ . Upon crossing the Feshbach resonance where  $a_{\phi\psi}^{-1}$  goes over to positive values, the attractive polaron evolves smoothly into a molecular bound state which follows the energy of the universal dimer,  $E_{\text{att}} \sim E_{\text{dim}} = -a_{\phi\psi}^{-2}(\alpha + 1)/2\alpha m_{\phi}$ .

Although it remains the stable ground state, the attractive polaron loses spectral weight in favor of a second feature which emerges at positive energies [cf. Figs. 4 and 5]. This ‘‘high-energy excitation’’ absorbs most of the spectral weight lost by the attractive polaron. Its positive energy indicates that it corresponds to a quasiparticle

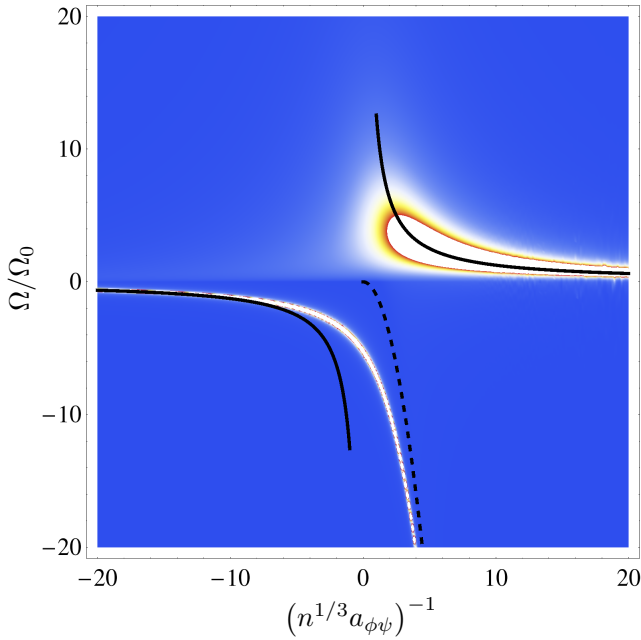


FIG. 2: Impurity spectral function  $A_{\text{pol}}(\Omega, \mathbf{p} = 0)$  in the non-selfconsistent T-matrix approximation with  $n^{1/3}a_{\phi\psi} = 0.1$ . Solid lines: weak coupling limit (valid for both branches)  $E \sim g_{\phi\psi}n$ . Dashed line: energy of the universal dimer in vacuum,  $E_{\text{dim}} \sim -1/m_{\phi}a_{\phi\psi}^2$ . Here and in all following plots, zero-width peaks are given a small artificial width to be visible on the graph.

interacting with the Bose gas via an effective repulsion, hence it is coined the repulsive Bose polaron in the following. The appearance of this repulsive branch has strong similarities to the “upper branch” present in the case of a two-component Fermi gas [61–63] and in particular the repulsive Fermi polaron [8, 64, 65]. Similarly to the latter case, the repulsive Bose polaron exists only at positive interspecies coupling and becomes a well-defined quasiparticle only for moderate to small values of the interaction constant  $a_{\phi\psi}$  as can be seen from its width  $\gamma$  shown in Fig. 4 (c). The appearance of the repulsive polaron suggests a simple physical picture where the impurity interacts with the bosons via a positive scattering length, resulting in a positive interaction energy. Indeed, we find that the energy of the repulsive polaron is well approximated by the mean field result  $E_{\text{rep}} \approx g_{\phi\psi}\rho_0$  wherever the quasiparticle peak is well defined. This picture, however, neglects the physical origin of the positivity of the scattering length which is the presence of a bound state in the spectrum. Indeed, as  $a_{\phi\psi}$  increases towards the Feshbach resonance, the corresponding lifetime rapidly becomes so short that a detailed experimental study of strongly repulsive polarons will be a major challenge.

In Appendix A we argue that when crossing the Feshbach resonance, there is actually a smooth crossover of the ground state from a polaronic to a bound molecule state, a picture which emerges naturally when consider-

ing the problem using a two-channel model instead of the one-channel model discussed here. Essentially, this crossover, which stands in clear contrast to the case of the Fermi polaron [54, 55, 66, 67], finds its origin in a hybridization of the molecular and the polaronic state due to the presence of the condensate [68]. This intuitive picture is corroborated by the fact that the effective mass of the attractive polaron crosses over from  $\alpha m_{\phi}$ , the mass of a single impurity, to  $(\alpha + 1)m_{\phi}$  which is the mass of a molecule made up of the impurity and one boson [cf. Fig. 5 (b)].

The behavior of the quasiparticles as a function of momentum, shown in Fig. 3, is qualitatively different on the two sides of the Feshbach resonance. For  $a_{\phi\psi} > 0$ , the attractive polaron’s momentum dependent effective mass increases with increasing momentum and its dispersion eventually follows the dispersion of the molecular state which reflects the polaron-to-molecule crossover also in the momentum domain. The onset of the scattering continuum happens at  $p^2/2\alpha m_{\phi}$  for  $p/\alpha m_{\phi} \leq c = \sqrt{g_{\phi\phi}n/m_{\phi}}$  (within the considered approximation, this statement is exact and reflects Landau’s critical velocity, cf. Appendix C) and crosses over to a molecule-like dispersion  $\sim p^2/2(\alpha + 1)m_{\phi}$  for larger momenta. The “dispersion law” of the continuum onset is determined by the onset of the imaginary part of the pair propagator and is thus independent of  $a_{\phi\psi}$  in the NSCT approach. As the attractive polaron peak approaches the molecule dispersion, it loses more and more of its spectral weight in favor of the repulsive polaron which gains spectral weight while its effective mass approaches  $\alpha m_{\phi}$ . At large momenta the repulsive polaron becomes a free particle as expected since at high momenta many-body fluctuations are suppressed and the impurity becomes ignorant of its environment. For negative  $a_{\phi\psi}$  the repulsive polaron is absent [cf. Fig. 3 (b)]. Here the attractive polaron has a spectral weight close to one and an effective mass close to  $\alpha m_{\phi}$  for all momenta. As a consequence, it eventually crosses the continuum onset and acquires a finite width. For large enough momenta, this width becomes negligible and the attractive polaron behaves as a free particle.

Our results depend only weakly on the boson–boson coupling  $g_{\phi\phi}$  which suggests to consider the simplifying limit  $g_{\phi\phi} \rightarrow 0$ . This limit should be understood in the following sense: while a finite value of  $g_{\phi\phi}$  is essential for the mechanical stability of the system, we are only interested in the effects of the Bose gas on the impurity, not the inverse. The limit  $g_{\phi\phi} \rightarrow 0$  is nothing but a mathematical commodity which actually means that boson–boson interaction are very weak but still sufficiently large to ensure stability [69, 70]. Carrying out the limit leads to important simplifications in the calculation. First, all Bose propagators become free particle propagators, thus eliminating the mathematically tricky Bogoliubov dispersion. Second, the loop diagram in Fig. 1 (b) vanishes identically, leaving only the mean field like contribution to the impurity selfenergy (7), i.e., the selfenergy is just proportional to the T-matrix  $\Gamma_{\phi\psi}$ .

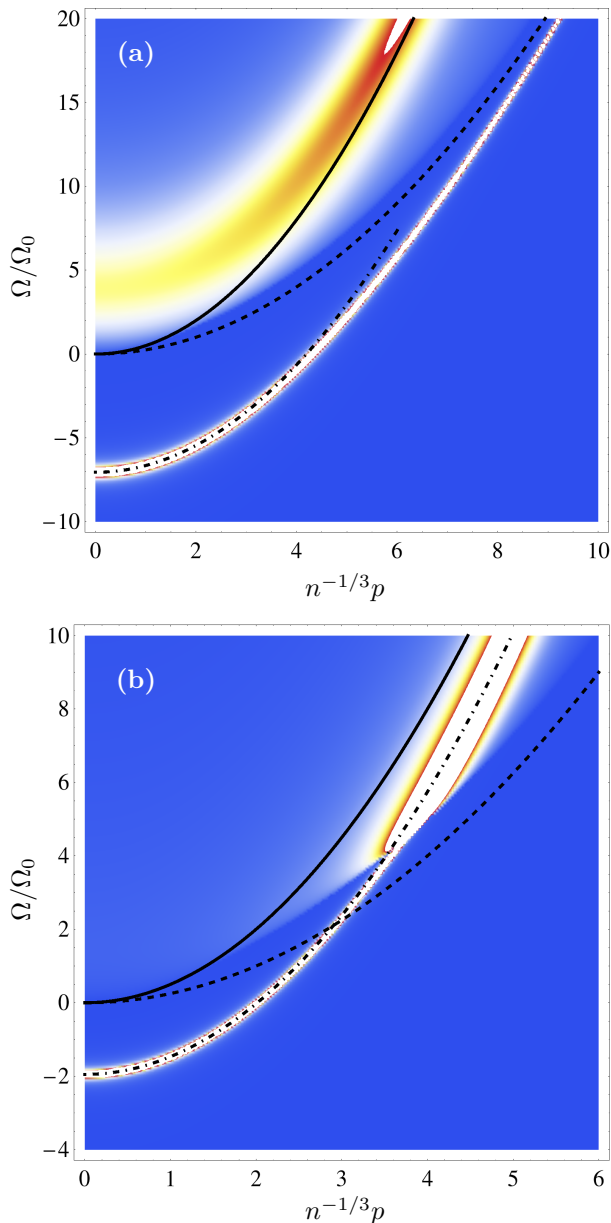


FIG. 3: Impurity spectral function  $A_{\text{pol}}(\Omega, \mathbf{p})$  as a function of frequency and momentum for (a)  $(n^{1/3}a_{\phi\psi})^{-1} = 1$  and (b)  $(n^{1/3}a_{\phi\psi})^{-1} = -5$ . In both graphs,  $n^{1/3}a_{\phi\phi} = 0.1$ . Solid line: free impurity dispersion. Dashed line: free molecule like dispersion. Dash-dotted line: dispersion according to the effective mass of the attractive polaron at  $p = 0$ . For positive  $a_{\phi\psi}$ , the attractive polaron peak gradually bends away from its dispersion at vanishing momentum, reflecting an increase in the momentum-dependent effective mass. At negative  $a_{\phi\psi}$ , the effective mass stays approximately constant as a function of momentum.

Furthermore, all anomalous contributions which are neglected in our calculation at finite  $g_{\phi\phi} > 0$  now indeed vanish. As already stated, in the approximation  $g_{\phi\phi} \rightarrow 0$  the in medium T-matrix is identical to the T-matrix in vacuum given in Eq. (13) up to the impurity's chemical potential absorbed in  $\Omega$ . Considering the simplicity of the selfenergy in the limit  $g_{\phi\phi} \rightarrow 0$ , it comes as a surprise that at vanishing momentum the resulting spectral function turns out to be almost identical to the one obtained for finite boson–boson interactions (cf. Figs. 4 and 5 for an explicit comparison of the quasiparticle properties for finite and vanishing boson–boson interactions). This is particularly remarkable since we deliberately chose the rather large value  $n^{1/3}a_{\phi\phi} = 0.1$  for the plots involving a finite boson–boson interaction.

The simplicity of the NSCT approximation with a non-interacting BEC allows to give some simple analytical relations between quasiparticle properties. The first relates the quasiparticle weight and the effective mass. In fact, since in this approximation the selfenergy is a function of  $\Omega - p^2/2(\alpha + 1)m_\phi$ , the effective mass can simply be expressed as

$$m^* = \frac{1 - \partial_\Omega \text{Re}\Sigma_\psi}{\frac{1}{\alpha} - \frac{1}{\alpha+1} \partial_\Omega \text{Re}\Sigma_\psi} \Big|_{E(p)} = \frac{\alpha(\alpha+1)}{Z + \alpha}. \quad (21)$$

One sees that the effective mass is strictly bounded by the impurity and the molecule mass and follows a smooth interpolation between the two as the scattering length is tuned across the resonance. This nicely reflects the crossover of the polaron to a molecule described in Appendix A. The quasiparticle weight  $Z$  and the effective mass  $m^*$  are shown as functions of  $a_{\phi\psi}^{-1}$  in Fig. 5. One may also determine the momentum at which the attractive polaron enters the excitation continuum at small negative  $a_{\phi\psi}$ . In this regime the polaron always has an effective mass close to  $\alpha m_\phi$  such that the polaron dispersion relation is well approximated by  $E_{\text{att}}(p) \approx g_{\phi\psi}n + p^2/2\alpha m_\phi$  while the onset of the continuum is exactly at  $p^2/2(\alpha+1)m_\phi$  (in contrast to the case of a non-zero  $g_{\phi\phi}$  discussed above). Consequently, the two intersect at  $p \approx \sqrt{-4\pi(\alpha+1)^2 n a_{\phi\psi}}$ . Finally, the energy of the attractive polaron may be calculated analytically. While the resulting expression is cumbersome, it permits to obtain the leading correction to the universal dimer energy which at small positive scattering lengths is given by  $E_{\text{att}} \sim (-1/a_{\phi\psi}^2 - 8\pi a_{\phi\psi}n)(\alpha+1)/2\alpha m_\phi$  [95].

The difference in the “dispersion” of the continuum onset depending on whether one assumes a finite  $g_{\phi\phi}$  or not is in fact the only qualitative difference that can be seen in the spectral function [cf. Fig. 6, where, in contrast to Fig. 3 (b), the continuum onset coincides with the free molecule dispersion marked by the dashed line]. As a consequence, while there is a visible deviation in the crossing between the attractive polaron and the continuum onset at positive  $a_{\phi\psi}$ , the relation (21) between  $Z$  and  $m^*$  is satisfied to a good approximation even for  $g_{\phi\phi} > 0$ . To summarize, within the chosen approximation scheme the influence of  $g_{\phi\phi}$ , in particular on quantities evaluated at



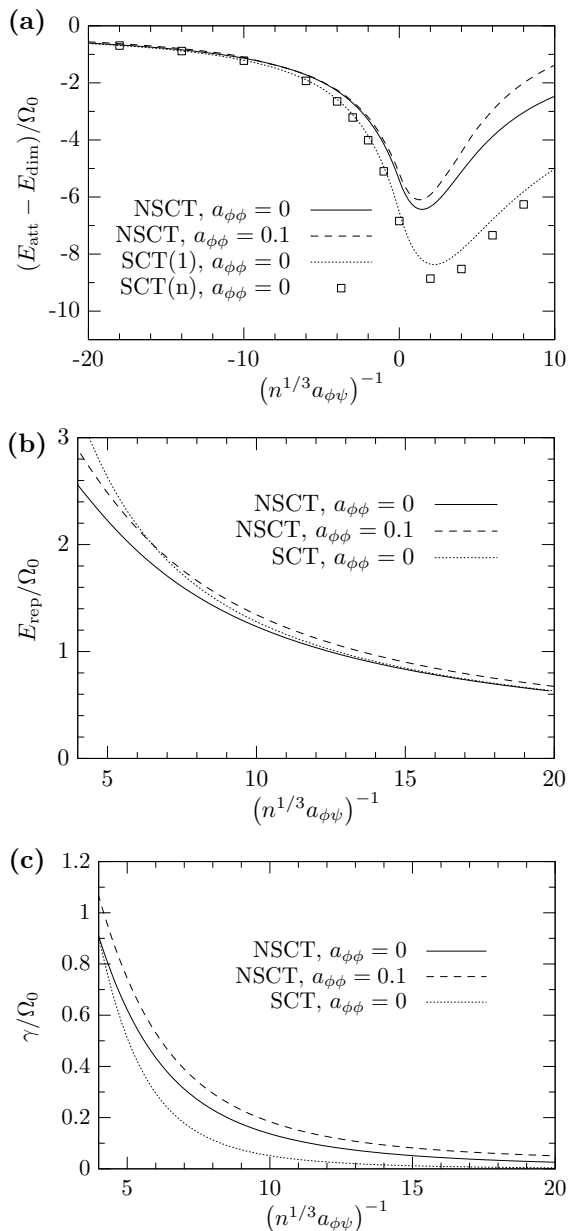


FIG. 4: Quasiparticle energies and width obtained in the non-selfconsistent T-matrix (NSCT) approach with both a finite and a vanishing boson–boson interaction, and the self-consistent (SCT) approach. In the latter case, the dotted line indicates the result after the first iteration of the selfconsistency loop while the individual dots denote the final value for 15 iterations when full selfconsistency of the T-matrix equations is reached. (a) Attractive polaron energy with the universal dimer binding energy  $E_{\text{dim}} = -\theta(a_{\phi\psi})/m_{\phi} a_{\phi\psi}^2$  subtracted. This representation accentuates the absolute difference between the values obtained in the various approximation schemes. The relative deviation is far smaller on the right of the minimum due to the large modulus of  $E_{\text{dim}}$ . (b) Energy of the repulsive polaron. The plot excludes low values of  $a_{\phi\psi}^{-1}$  where the repulsive polaron is not properly defined. (c) Quasiparticle width of the repulsive polaron for the same range of values of  $a_{\phi\psi}^{-1}$ .

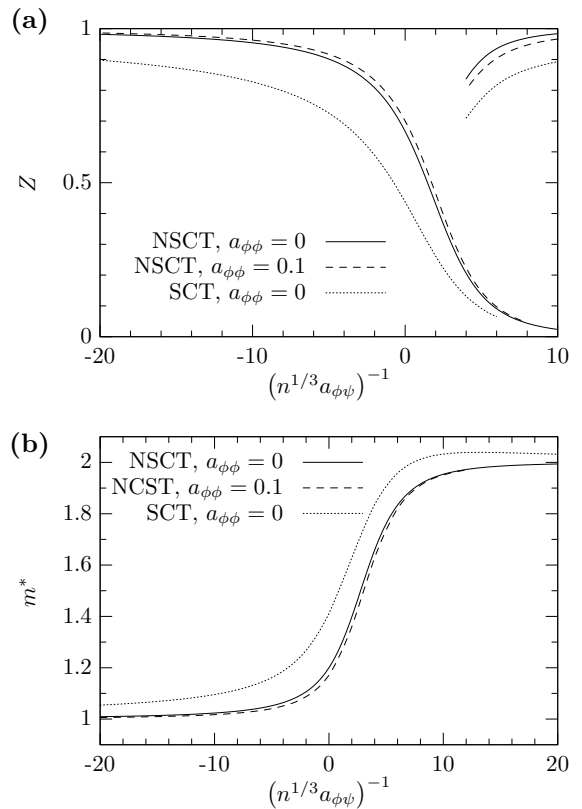


FIG. 5: (a) Quasiparticle weights for both branches (the lines on the upper right of the graph correspond to the repulsive polaron). (b) Effective mass of the attractive polaron. Parameters and line styles are as in Fig. 4.

vanishing momentum, is almost invisible in spite of the very large value  $n^{1/3} a_{\phi\psi} = 0.1$  used in the data shown before.

#### IV. SELFCONSISTENT T-MATRIX APPROXIMATION

In the NSCT approach the backaction of the impurity selfenergy on the in-medium T-matrix is neglected since only bare impurity Green’s functions appear on the right-hand side of the T-matrix equation depicted in Fig. 1 (c). In this Section we include this feedback by solving the Bose polaron problem using a *selfconsistent* T-matrix (SCT) approach where the thin impurity line on the right-hand side of Fig. 1 (c) becomes bold, i.e., the bare impurity propagator is replaced by its dressed counterpart determined by Dyson’s equation. Motivated by our observation that within our T-matrix approach the inclusion of a finite boson–boson repulsion yields only quantitative corrections to the results [96], we only consider the limit  $g_{\phi\phi} \rightarrow 0$  in the following.

In the context of ultracold gases in the continuum, the selfconsistent T-matrix approach has been employed by



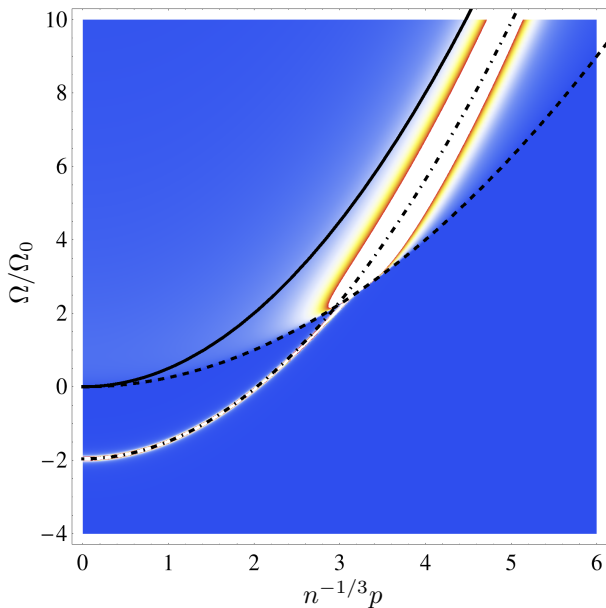


FIG. 6: Spectral function  $A_{\text{pol}}(\Omega, \mathbf{p})$  for  $a_{\phi\phi} = 0$ , all other parameters are as Fig. 3 (b). Note that here the continuum onset coincides with the dashed line indicating the free molecule like dispersion. The point where the polaron peak acquires a finite width is shifted accordingly.

Haussmann and coworkers for the study of the BEC–BCS crossover both for thermodynamic and dynamical quantities [71–74]. For instance, their prediction for the equation of state is in very good agreement with experiments [75] and state of the art bold diagrammatic Monte-Carlo calculations [76] in both the superfluid and the normal phase of the balanced Fermi gas. As we will see, the inclusion of selfconsistency leads to important quantitative changes in the ground state properties as well as qualitative changes in the excitation spectrum.

The inclusion of the dressed impurity Green’s function leads to the modified many-body T-matrix equation

$$\frac{1}{\Gamma_{\phi\psi}(i\omega, \mathbf{p})} = g_{\phi\psi}^{-1} + \int_{\mathbf{k}} \left\{ \int_{\nu} G_{\phi}^{(0)}[i(\omega - \nu), \mathbf{p} - \mathbf{k}] \times \frac{1}{i\nu - \frac{\mathbf{k}^2}{2\alpha} + \mu_{\psi} - \rho_0 \Gamma_{\phi\psi}(i\nu, \mathbf{k})} - \frac{2\alpha m_{\phi}}{(\alpha + 1)\mathbf{k}^2} \right\}. \quad (22)$$

In contrast to the NSCT approach, this equation includes the virtual excitation of an arbitrary number of bosons from the condensate. Unlike in Eq. (8), the unknown function  $\Gamma_{\phi\psi}(i\omega, \mathbf{p})$  now appears (in a non-linear way) on both sides of the integral equation which complicates the calculation significantly. We perform this calculation using imaginary frequencies because the resulting Green’s functions are smooth functions of the frequency, which makes them easier to handle than their counterparts at real frequencies—the latter may develop non-analytic features such as kinks as we have seen in the

previous Section. While the angular part of the momentum integration can be performed analytically, there is no evident way to do so for the frequency integration because the analytical structure of the T-matrix  $\Gamma_{\phi\psi}$  on the right-hand side is a priori unknown. This leaves us with two integrals that have to be evaluated numerically.

The mathematical structure of Eq. (22) resembles the renormalization group equations obtained for the pair propagator in the study of the Fermi polaron using the functional renormalization group [8]. Thus, we may use a similar numerical scheme to calculate the right-hand side of this equation. To this end, we discretize the T-matrix on a grid in momentum and frequency space  $(i\omega_k, p_l)$ . Due to spatial isotropy, the grid depends only on frequencies and absolute momenta. Furthermore, we exploit the fact that for high frequencies and momenta the many-body T-matrix reduces to the T-matrix in vacuum to a very good approximation. The maximum extent of the resulting finite grid is chosen such that the error due to this truncation is smaller than the accuracy of the final results. The latter is limited by the finite number of grid points as well as the finite number of steps used to solve Eq. (22) iteratively. The chosen grid contains  $\mathcal{O}(10^3)$  grid points. The frequency and momentum integration in Eq. (22) is performed using a bicubic spline interpolation of the numerical data as done in [8].

In order to solve Eq. (22) selfconsistently we rely on an iterative scheme. We start by solving this equation for an initial choice  $\Gamma_{\phi\psi}^{(0)}$  of the T-matrix appearing on the right-hand side given by the non-selfconsistent T-matrix obtained in the previous Section. The evaluation of the right-hand side then yields an “improved” T-matrix  $\Gamma_{\phi\psi}^{(1)}$  which in turn is reinserted into the right-hand side of Eq. (22). This yields the next iteration  $\Gamma_{\phi\psi}^{(2)}$  and so on. The process is iterated until convergence to a numerically stable result is reached. We find that  $n \lesssim 10$  iterations are typically sufficient. To verify the numerical stability of the final result, however, we carry on until up to  $n = 20$  iterations.

From the T-matrix  $\Gamma_{\phi\psi}^{(n)}$  in the  $n$ th step of this “selfconsistency loop” we calculate the improved, dressed impurity Green’s function  $G_{\psi}^{(n)}$  via Dyson’s equation depicted in Fig. 1 (a). In the numerical solution using imaginary frequencies, it is of utmost importance to adjust the impurity chemical potential  $\mu_{\psi}$  to a value that guarantees that the impurity atom does not have a finite occupation in the final iteration, i.e., one has to satisfy the condition

$$\left[ G_{\psi}^{(0)}(i\omega = 0, \mathbf{p}; \mu_{\psi}) \right]^{-1} - \rho_0 \Gamma_{\phi\psi}^{(n)}(i\omega = 0, \mathbf{p}; \mu_{\psi}) \leq 0 \quad (23)$$

for all  $\mathbf{p}$ . In fact, if we require Eq. (23) to be an equality with the choice of  $\mu_{\psi} = \mu_{\text{pol}}$  at  $\mathbf{p} = 0$ , this uniquely determines the ground state energy of the attractive polaron via the basic definition of the chemical potential,  $\mu_{\text{pol}} = E(N_{\psi} + 1) - E(N_{\psi})$ , where  $N_{\psi} = 1$  for the impurity problem, hence  $E_{\text{att}} = \mu_{\text{pol}}$ . The energies obtained

from the selfconsistent T-matrix approach are shown in Fig. 4 along with the results of the NSCT approximation. Specifically at unitarity where changes with respect to the NSCT schema are particularly strong, we find  $E_{\text{att}}/\Omega_0 = -6.84(1)$  while the NSCT approach yields  $E_{\text{att}}/\Omega_0 = -5.390$ . We see that the changes are of the order of 25 percent around unitarity.

To study the impact of selfconsistency on the excitation spectrum of the system, we have to perform an analytical continuation of the impurity Green's function to real frequencies. Although this is in principle possible, it would require the analytical continuation from a finite, discrete set of numerical data which is a mathematically ill-defined problem. In order to avoid the related complications and yet obtain fairly precise results, we make use of the observation that the by far largest effect of selfconsistency arises already in the first iteration [cf. the dotted line in Fig. 4 (a)]. Thus we expect that all major aspects of the impact of selfconsistency on the impurity spectral function are already present at this stage. The numerical cost of this first iteration is modest. One only has to calculate the integral appearing in Eq. (9), but with the bare Fermi propagator replaced by

$$G_{\psi}^{(1)}(\Omega, \mathbf{p}) = \frac{1}{\Omega - \frac{\mathbf{p}^2}{2m_{\psi}} - \rho_0 \Gamma_{\phi\psi}^{\text{NSCT}}(\Omega, \mathbf{p}) + i0^+} \quad (24)$$

where  $\Gamma_{\phi\psi}^{\text{NSCT}}$  is the non-selfconsistent T-matrix we obtained in the previous Section, cf. Eqs. (8) and (9). Since the integrand is known analytically, the frequency integration and subsequent continuation to real frequencies may be carried out analytically so that only the momentum integral has to be done numerically.

The qualitative changes following from this scheme with respect to the non-selfconsistent one can be seen in Fig. 7. The continuum onset is pulled to negative energies and now follows the curve which in the non-selfconsistent approximation is described by the polaron peak. A similar behavior has been found for the molecule spectral function in a renormalization group study of the Fermi polaron [8]. This may be seen as a further indication of the Bose polaron being hybridized with the molecule, cf. Appendix A. Moreover, we observe a strong suppression of both the attractive and the repulsive polaron's spectral weight. This large suppression, however, does not come as a surprise. Indeed, by solving Eq. (22) self-consistently we incorporate more fluctuations which entangle the impurity with the bosons' degrees of freedom. This loss of spectral weight in the attractive polaron is compensated by a transfer of weight to excited continuum states which is facilitated by the reduced excitation gap as compared to the NSCT approach. The substantial reduction of the quasiparticle weight is accompanied by changes to the effective mass of a similar magnitude. In the selfconsistent calculation the effective mass is no longer related to the quasiparticle weight by the simple relation (21) and takes values larger than  $(\alpha + 1)m_{\phi}$ . However, apart from a small upward shift, it still essentially follows its behavior from the NSCT approximation

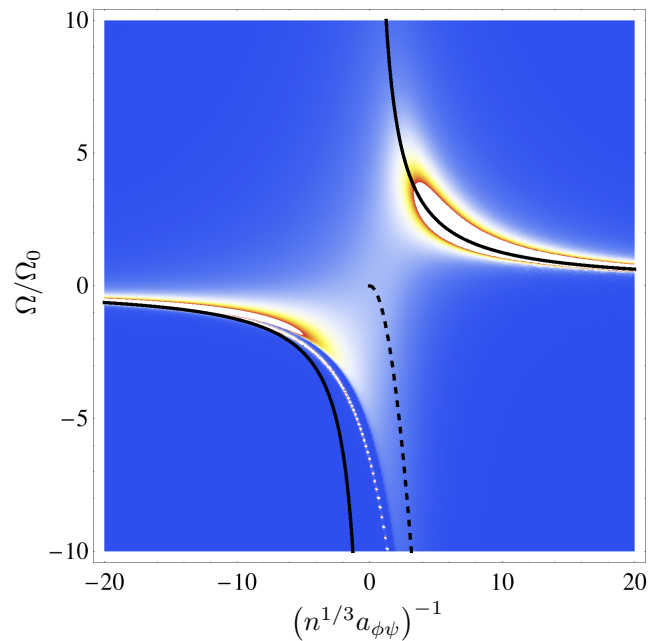


FIG. 7: Polaron spectral function calculated using the self-consistent scheme discussed in Section IV. The black lines are identical to the ones in Fig. 2. Note how the continuum of excitations now follows the attractive polaron peak.

[cf. Fig. 5 (b)]. The repulsive polaron is shifted to slightly higher energies [cf. Fig. 4] while its quasiparticle width is substantially reduced with respect to the NSCT result for all but the strongest interspecies interactions.

Further changes can be seen when one considers the momentum dependence of the impurity spectral function which is shown in Fig. 8 for two different values of the interspecies coupling. The most prominent difference appears for positive values of  $a_{\phi\psi}^{-1}$  [Fig. 8 (a)] where the attractive polaron peak touches the continuum and dies out rapidly instead of running parallel to it as it does in the NSCT approximation. The qualitative behavior of the repulsive polaron, however, remains unchanged, showing a smooth interpolation from a very broad peak at low momenta to a sharp peak with an effective mass of  $\alpha m_{\phi}$  towards higher momenta. The changes with respect to the NSCT approach are less pronounced for negative values of  $a_{\phi\psi}^{-1}$  [Fig. 8 (b)]. Here one only notices that when the attractive polaron pole enters the continuum—which happens at lower momenta than in the NSCT approximation due to the continuum's being pulled to negative frequencies—the latter is gradually absorbed by the former. Hence, within the SCT approach, the attractive polaron becomes subject to damping above a critical momentum for *any* interspecies interaction strength.

## V. CONCLUSION AND OUTLOOK

We have determined the excitation spectrum of an impurity immersed in a homogeneous BEC. We find that this spectrum is dominated by two branches, the attractive and repulsive Bose polaron. The attractive polaron is a stable quasiparticle at negative energies which exists for all interspecies couplings. It exhibits a crossover from a weakly dressed polaron to a molecule as one crosses the Feshbach resonance. This can be understood in terms of its hybridization with a molecular state due to the BEC. The repulsive polaron emerges as a metastable quasiparticle on the  $a_{\phi\psi}^{-1} > 0$  side of the Feshbach resonance. While it is long-lived for small scattering lengths  $a_{\phi\psi}$ , its lifetime becomes exceedingly small as the Feshbach resonance is approached. The essence of the problem can already be captured by a non-selfconsistent calculation using a vanishing boson–boson coupling constant. The most important correction to this simple picture is given by the multiple excitation of bosons from the condensate, which we account for by the selfconsistent incorporation of the selfenergy feedback into the T-matrix equation. We predict various quasiparticle properties of the attractive and repulsive polaron which can be tested in future experiments. For instance, radiofrequency experiments permit to measure not only the excitation energies [37], but also the quasiparticle weight and width. The latter two can be inferred from a shift in the Rabi frequency and the damping of Rabi oscillations, respectively [9]. The effective mass may in turn be determined using momentum-resolved photoemission or Raman spectroscopy [7, 36, 38, 77].

It is an interesting question what happens on time scales longer than those relevant for inverse rf experiments. For instance, the repulsive polaron exhibits a positive energy which decreases when  $na_{\phi\psi}^3$  is lowered. Thus, in an experimental situation with a trapped BEC, the repulsive polaron can minimize its energy by moving to a region of lower density [15]. The fact that this tendency towards phase separation happens for any positive  $a_{\phi\psi}$  is in stark contrast to the case of the repulsive Fermi polaron. In the latter, phase separation—which here may also be seen as a transition towards a ferromagnetic phase—only happens for interaction strengths above a critical value due to the competition between kinetic and interaction energy [8, 65]. For the Bose polaron, the process of phase separation is itself in competition with the tendency towards self-localization accompanied by a local deformation of the BEC. Concerning the study of such dynamical phenomena, our calculation can be seen as the derivation of an effective field theory for the repulsive Bose polaron which includes quasiparticle properties such as a finite lifetime and an effective momentum-dependent interaction. Starting from the corresponding equations of motion, the time evolution from the initial out-of-equilibrium state towards self-localization or phase separation may now be studied. Note that our discussion so far ignores the effects of three-body recombina-

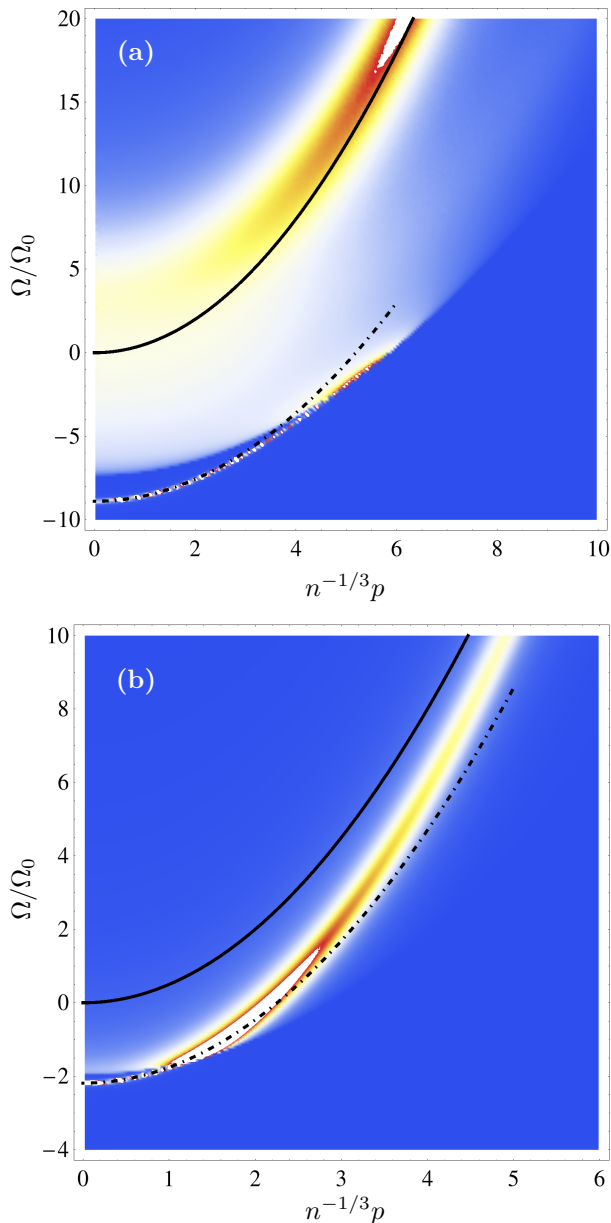


FIG. 8: Polaron spectral function calculated using the self-consistent scheme discussed in Section IV as a function of momentum and frequency. The black lines have the same meaning as in Fig. 3. (a)  $(n^{1/3}a_{\phi\psi})^{-1} = 1$ . Note how the attractive polaron peak is “annihilated” when it touches the continuum. (b)  $(n^{1/3}a_{\phi\psi})^{-1} = -5$ . The continuum practically merges with the peak for higher momenta.

tion due to Efimov physics [78]. Even in our inverse rf spectroscopy scenario, the latter is not completely suppressed. In the case of the repulsive polaron, one may however even utilize the Efimov effect to suppress losses by exploiting the minima in the three-body recombination which are due to the destructive interference of decay channels [79]. In fact, it poses an interesting question on its own how Efimov physics is affected by medium effects [80] such as the hybridization of the impurity with the molecular state.

Finally, it would be interesting to investigate the possibility of an alternative representation of the Bose polaron. In the Fermi polaron problem the NSCT approach leads to equations which are formally equivalent to the equations obtained from a simple variational wave function ansatz [53]. This ansatz describes the Fermi polaron as a bare impurity dressed by a single particle-hole fluctuation. We expect that such a mapping from diagrams to a variational wave function exists as well in the present case of the Bose polaron.

### Acknowledgments

We thank Wilhelm Zwerger for suggesting the problem and for careful reading of this manuscript. We also acknowledge helpful discussions with Marcus Barth, Eugene Demler, Tilman Enss, Francesco Piazza and Alessio Recati. This work has been supported by the DFG Forschergruppe 801.

### Appendix A: Hybridization, molecule Green's function and polaron-to-molecule crossover

In experiments, large scattering lengths can be achieved by the use of Feshbach resonances. Here the dependence of the energy level of a closed-channel molecule on an external magnetic field is exploited to obtain arbitrarily large scattering lengths when the state approaches the open-channel scattering threshold. The basic physics of a Feshbach resonance can be described by the use of a simple two-channel model which explicitly includes the molecular state as a dynamical degree of freedom. While detailed accounts on the physics of the two-channel model in the context of Fermi- and Bose gases can be found in literature [6, 39, 81–83], we will focus here on the particularities which arise in the mixed Bose-impurity system due to the presence of the condensate. In particular, the study of the two-channel model allows to connect our results for the T-matrix  $\Gamma_{\phi\psi}$ , obtained in the single-channel model employed so far, with the propagator of the molecule. In this context we highlight the differences in comparison to the case of a Fermi polaron. Specifically, in a description of the Fermi polaron in the limit

of open-channel dominated Feshbach resonances, the T-matrix can be interpreted as the molecule propagator when physics close to the resonance is considered. The spectral function of the molecule is then simply proportional to the imaginary part of the T-matrix. While in the Fermi polaron problem this identification even allows for a qualitatively correct description of the polaron-to-molecule transition present in this system [48, 66, 84], we show in this Appendix how such a simple identification of the T-matrix with the molecule propagator fails in the context of the Bose polaron where no transition but rather a crossover occurs.

The two-channel model describing a Bose polaron close to a Feshbach resonance of arbitrary width [39] is given by

$$S = \int d\tau \int d^3x \left\{ \varphi_{\mathbf{x},\tau}^* \left( \partial_\tau - \frac{1}{2m_\phi} \nabla^2 - \mu_\phi \right) \varphi_{\mathbf{x},\tau} + \psi_{\mathbf{x},\tau}^* \left( \partial_\tau - \frac{1}{2\alpha m_\phi} \nabla^2 - \mu_\psi \right) \psi_{\mathbf{x},\tau} + \xi_{\mathbf{x},\tau}^* \left( \partial_\tau - \frac{1}{2(\alpha+1)m_\phi} \nabla^2 + \nu_M \right) \xi_{\mathbf{x},\tau} + \frac{g_{\phi\psi}}{2} |\varphi_{\mathbf{x},\tau}|^4 + h \left( \xi_{\mathbf{x},\tau}^* \psi_{\mathbf{x},\tau} \varphi_{\mathbf{x},\tau} + \psi_{\mathbf{x},\tau}^* \varphi_{\mathbf{x},\tau} \xi_{\mathbf{x},\tau} \right) \right\}, \quad (\text{A1})$$

where the field  $\xi$  describes the molecular state in the closed channel which is a composite state of an impurity and a boson. The interaction between the impurity  $\psi$  and the bosons  $\varphi$  is mediated by the exchange of a molecule  $\xi$  which couples via the conversion coupling  $h$  to the impurity and the bosons. The analysis of the few-body physics governed by Eq. (A1) shows that  $h$  is connected to the experimentally accessible characteristic width of the Feshbach resonance  $r^*$  via  $h^2 \sim 1/r^*$ . While the limit  $h \rightarrow \infty$  describes so-called open-channel dominated Feshbach resonances, a resonance is termed closed-channel dominated in the limit  $h \rightarrow 0$ .

The molecule is a physically propagating degree of freedom and as such is supplemented by a dynamical propagator already on the level of the classical action (A1). The parameter  $\nu_M$  denotes the detuning of the energy of the bare molecular state with respect to the atom scattering threshold and depends on the external magnetic field [6, 39, 81–83]. The action (A1) is quadratic in the field  $\xi$ , and by integrating out  $\xi$  in the path integral one easily verifies that the two-channel model is equivalent to the single-channel model (1) in the open-channel dominated limit where  $h \rightarrow \infty$ . In this limit the momentum dependence of  $\xi$  becomes irrelevant and one finds the identification  $\tilde{g}_{\phi\psi} = -h^2/\nu_M$ .

If we treat the bosons in the Bogoliubov approximation and neglect the backaction of the impurity on the condensate, we obtain

$$S_{\text{eff}} = \int_p \left\{ \frac{1}{2} \begin{pmatrix} \phi_p^* \\ \phi_{-p} \end{pmatrix} \begin{pmatrix} -[G_\phi^{(0)}(-p)]^{-1} & g_{\phi\phi\rho_0} \\ g_{\phi\phi\rho_0} & -[G_\phi^{(0)}(p)]^{-1} \end{pmatrix} \begin{pmatrix} \phi_p \\ \phi_{-p}^* \end{pmatrix} + \begin{pmatrix} \psi_p^* \\ \xi_p^* \end{pmatrix} \begin{pmatrix} -[G_\psi^{(0)}(p)]^{-1} & h\sqrt{\rho_0} \\ h\sqrt{\rho_0} & -[G_\xi^{(0)}(p)]^{-1} \end{pmatrix} \begin{pmatrix} \psi_p \\ \xi_p \end{pmatrix} \right\} + h \int_x (\xi_x^* \psi_x \phi_x + \psi_x^* \phi_x^* \xi_x), \quad (\text{A2})$$

where  $G_\psi^{(0)}$  is the bare impurity propagator as used in the main body of the article, and  $G_\xi^{(0)} = [i\omega - \mathbf{p}^2/2(\alpha + 1)m_\phi - \nu_M]^{-1}$  is the bare molecule propagator. From this form of the action, one may directly read off the mean field (fermionic) propagators

$$G_\psi(\Omega, \mathbf{p}) = \frac{G_\psi^{(0)}(\Omega, \mathbf{p})}{1 - h^2 \rho_0 G_\xi^{(0)}(\Omega, \mathbf{p}) G_\psi^{(0)}(\Omega, \mathbf{p})}, \quad (\text{A3})$$

$$G_\xi(\Omega, \mathbf{p}) = \frac{G_\xi^{(0)}(\Omega, \mathbf{p})}{1 - h^2 \rho_0 G_\xi^{(0)}(\Omega, \mathbf{p}) G_\psi^{(0)}(\Omega, \mathbf{p})}$$

In the limit  $\rho_0 \rightarrow 0$ , i.e., in absence of a condensate, these propagators reduce to their usual bare form also encountered for instance in the context of the Fermi polaron close to a narrow Feshbach resonance [9, 85, 86]. In the presence of a BEC, however, the propagators are hybridized [68] which constitutes a fundamental difference between pure Fermi–Fermi and Bose–Fermi mixtures already on the classical (mean field) level.

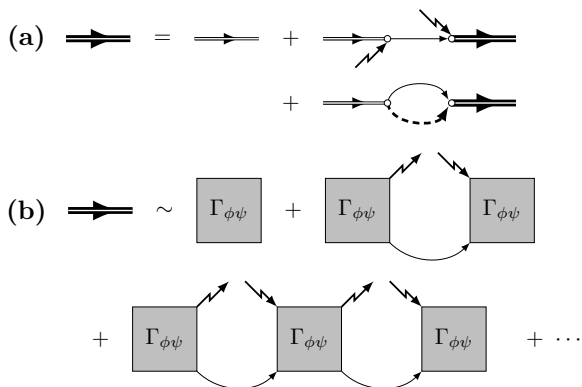


FIG. 9: (a) Dyson's equation for the molecule propagator in the two-channel model (A2) in a T-matrix like approximation. Double lines denote the molecule propagator and open circles represent the atom–molecule conversion coupling  $h$ . (b) Diagrammatic representation of the molecule propagator within a single-channel description of the Bose polaron. Note that in order to establish the correspondence  $\mathcal{G}_\xi \leftrightarrow \Gamma_{\phi\psi}$ , one has to assume implicit conversion coupling vertices at both ends of the propagator line on the left-hand side.

While the results of the NSCT approximation presented in Section III can be recovered in the limit  $h \rightarrow \infty$ ,

the two-channel model also allows to generalize these results to resonances of arbitrary width. Although this poses an interesting problem on its own, we focus here on the question of how the presence of hybridization alters the identification of the molecule with the T-matrix which is simply a proportionality in the Fermi polaron problem close to a broad Feshbach resonance [66, 67, 84–88]. To study this question, we calculate the molecular Green's function  $\mathcal{G}_\xi$  which is renormalized by the ladder diagram depicted in Fig. 9 (a). This leads to

$$[\mathcal{G}_\xi(\Omega, \mathbf{p})]^{-1} = \Omega - \frac{\mathbf{p}^2}{2(\alpha + 1)m_\phi} - h^2 \rho_0 G_\psi^{(0)}(\Omega, \mathbf{p}) + h^2 \Gamma_{\phi\psi}^{-1}(\Omega, \mathbf{p}), \quad (\text{A4})$$

where  $\Gamma_{\phi\psi}$  appears upon the evaluation of the particle-particle loop diagram depicted in Fig. 9 (a). We now take the limit of an open-channel Feshbach resonance  $h \rightarrow \infty$ . This results in the irrelevance of the dynamical part in the first line of Eq. (A4) and  $\mathcal{G}_\xi$  reduces to

$$h^2 \mathcal{G}_\xi(\Omega, \mathbf{p}) = \frac{\Gamma_{\phi\psi}(\Omega, \mathbf{p})}{1 - \rho_0 \Gamma_{\phi\psi}(\Omega, \mathbf{p}) G_\psi^{(0)}(\Omega, \mathbf{p})}. \quad (\text{A5})$$

From this expression the correspondence between  $\Gamma_{\phi\psi}$  and the molecule propagator within a single-channel description becomes apparent. It is given by the resummation of the diagrammatic series depicted in Fig. 9 (b). This diagrammatic structure does not exist in the Fermi polaron problem as it is solely a consequence of the hybridization originating from the presence of the condensate. Note that the expression on the right-hand side of Eq. (A5) is precisely the quantity called  $T$  (as opposed to  $\Gamma$ ) by the authors of [89, 90]. Hence, their distinction between these two quantities may also be seen as one between the T-matrix and the molecule propagator.

The derivation of the spectral function of the propagating degrees of freedom necessitates the diagonalization of the full *matrix* Green's function which mixes the fermionic and molecular states in the Nambu spinor  $\chi = (\psi, \xi)^T$ . In consequence the resulting full Green's functions for the impurity and the molecule exhibit the same pole structure which is the essence of the hybridization of the molecule with the impurity degree of freedom. The inspection of the denominator in (A5) now reveals that it is identical to the denominator of the impurity Green's function  $G_\psi^{(1)}$  in Eq. (24) which is obtained

in the approximation which only takes into account the repeated impurity–condensate scattering. Hence, the molecule and the polaron have indeed the same pole structure and we have successfully established a consistent relation between the molecule propagator and the T-matrix in a single-channel description.

The description in terms of the Nambu spinor  $\chi$  also allows to characterize the nature of the eigenstates with respect to which the corresponding matrix propagator becomes diagonal in field space. This diagonalization is achieved using a transformation matrix  $U(\theta) \in \text{SO}(2)$ , where  $\theta \in [0, \pi/2]$  is a scattering length dependent mixing angle. For  $\theta = 0$ , the matrix Green’s function is diagonal and the fields  $\psi$  and  $\xi$  are its eigenstates. For finite values of  $\theta$ , however, the eigenstates are superpositions of the two fields. In dependence on the scattering length, the tangent  $\tan(2\theta)$  falls off to zero for weak attraction while it has a pole close to unitarity. As a consequence of this pole, the eigenstate which starts as the impurity state on the side of small negative  $a_{\phi\psi}$  ends up as the molecular state on the side of small positive  $a_{\phi\psi}$  and vice versa, in agreement with the intuitive picture of a smooth polaron-to-molecule crossover.

## Appendix B: Regularization of the boson–boson interaction

In this Appendix we comment on the regularization of the boson–boson interaction and on how the bare coupling constant  $\tilde{g}_{\phi\phi}$  connects to the scattering length  $a_{\phi\phi}$  which parametrizes the s-wave scattering amplitude  $f(k)$  in the low-energy limit. Note that the following arguments apply equally well to the boson–impurity coupling  $\sim \tilde{g}_{\phi\psi}$ . The relation between  $\tilde{g}_{\phi\phi}$  and  $a_{\phi\phi}$  is obtained by considering the two-body scattering problem which in principle requires a rigorous treatment of the boson–boson interaction by solving the Lippmann–Schwinger equation (LSE) using the actual two-body interaction potential as an input. Solving this problem is in general very difficult—in most cases not even the two-body potential is known exactly—but fortunately it is unnecessary when one is only interested in physics at low collision energies where the physics is described by the scattering length  $a_{\phi\phi}$  alone. Indeed, in the case of low-energy scattering the solution of the LSE can be viewed as a mapping of the two-body potential on this single parameter  $a_{\phi\phi}$ . Exploiting this consequence of universality, it is possible to choose a representative out of the class of interaction potentials leading to the same value of  $a_{\phi\phi}$ . A particularly convenient choice is the contact interaction used in our model (1).

Having properly set up the microscopic model (1), we are now interested in the connection between  $a_{\phi\phi}$  and  $\tilde{g}_{\phi\phi}$ . To this end, it is sufficient to consider the scattering amplitude  $f(k)$  at vanishing scattering momentum  $\mathbf{k}$ . In this limit the evaluation of the LSE yields (in this

Appendix we use units where  $m_\phi = 1$ )

$$\frac{1}{\Gamma_{\phi\phi}^{2\text{B}}(0, \mathbf{0})} = \frac{1}{4\pi a_{\phi\phi}} = \frac{1}{\tilde{g}_{\phi\phi}} + \int \frac{d^3q}{(2\pi)^3} \frac{g(q)}{q^2} \quad (\text{B1})$$

where we used the relation between the T-matrix and the scattering amplitude  $f(k) = -\Gamma_{\phi\phi}^{2\text{B}}(\omega = \mathbf{k}^2, \mathbf{0})/4\pi$  for two atoms scattering in the center-of-mass frame with momenta  $\mathbf{k}$  and  $-\mathbf{k}$ . In the case of contact interactions,  $g(q) = 1$  so that the second term in Eq. (B1) diverges and has to be regularized. The appearance of this divergency is however a pure artifact which originates from the choice of the rather unphysical contact interaction. Any typical interaction potential of a finite range  $r_0$  would automatically lead to a regularization of the integral at a momentum scale  $\Lambda$  of the order of the inverse range  $1/r_0$ . In Eq. (B1) this is mimicked by the presence of the function  $g(q)$ . The regularization at high momenta can in particular be realized by introducing a sharp momentum cutoff at the scale  $\Lambda$  which for cold atoms is then of the order of the inverse van-der-Waals length  $1/l_{\text{vdw}}$ . Carrying out the integral in Eq. (B1) one obtains

$$\frac{1}{\tilde{g}_{\phi\phi}} = \frac{1}{4\pi a_{\phi\phi}} - c\Lambda, \quad (\text{B2})$$

where  $c$  is a numerical factor which for the choice of a sharp momentum regulator  $g(q) = \theta(\Lambda - q)$  is given by  $c = 1/(2\pi^2)$ .

The simple Eq. (B2) represents the connection between  $a_{\phi\phi}$  and  $\tilde{g}_{\phi\phi}$  we sought after and from which a few subtleties in the renormalization procedure of the coupling  $\tilde{g}_{\phi\phi}$  become apparent. For instance, assuming a microscopically repulsive interaction, i.e.,  $\tilde{g}_{\phi\phi} > 0$ , we directly see that in the zero-range limit  $r_0 \rightarrow 0$ , i.e.,  $\Lambda \rightarrow \infty$ , the scattering length  $a_{\phi\phi}$  is bound to be zero which merely reflects the fact that any repulsive potential, no matter how strong, can feature a scattering length at most as large as the range of the potential [91]. The only way to recover a finite scattering length for repulsive interactions is thus to keep  $\Lambda \sim 1/r_0$  finite. From Eq. (B2) it is then apparent that if the Bose gas is very weakly interacting with a small scattering length  $a\Lambda \ll 1$ , one may neglect the term proportional to  $\Lambda$  which yields the commonly used relation  $\tilde{g}_{\phi\phi} = 4\pi a_{\phi\phi}$  we also employed in the Bogoliubov approximation of the Bose gas discussed in Section II.

The above argument ignores the fact that cold atoms are always interacting via microscopically *attractive* interactions. Thus,  $\tilde{g}_{\phi\phi}$  is bound to be negative, no matter the sign of  $a_{\phi\phi}$ . Although making the matter more difficult, attractive interactions also lead to far richer physics. For instance, by virtue of Eq. (B2) it is possible to achieve any desired scattering length  $a_{\phi\phi}$  by fine-tuning  $\tilde{g}_{\phi\phi}$  as function of the range of the potential  $r_0 \sim 1/\Lambda$ . Furthermore, for attractive interactions it is possible to take the zero-range limit  $\Lambda \rightarrow \infty$  while still retaining an arbitrary value of  $a_{\phi\phi}$ . This also reflects the presence of universality: by adjusting  $\tilde{g}_{\phi\phi}$  according to Eq. (B2) and



afterwards sending  $\Lambda$  to infinity, all information about the short-range details are hidden in the single parameter  $g_{\phi\phi}$ .

### Appendix C: Analytical calculation of the T-matrix with finite boson–boson interaction

With some effort, it is possible to calculate an analytical expression for the T-matrix even when including the Bogoliubov propagators of the weakly interacting Bose gas instead of their bare counterparts. The calculation is most conveniently done in units where masses are measured in units of the boson mass  $m_\phi$ , energies in units of  $\mu_\phi = g_{\phi\phi}\rho_0$ , and consequently length scales in units of the healing length  $1/\sqrt{g_{\phi\phi}\rho_0}$ . In these units, the pair propagator  $L(\Omega, \mathbf{p})$  only depends on  $\Omega$  and  $p = |\mathbf{p}|$  which simplifies the notation considerably. To restore the units used in the main part of this article where we set the typical interparticle distance  $\sim n^{-1/3}$  to one instead of the healing length, one has to use the substitution

$$L(\Omega, p) \mapsto \sqrt{g_{\phi\phi}} L\left(\frac{\Omega}{g_{\phi\phi}}, \frac{p}{\sqrt{g_{\phi\phi}}}\right). \quad (\text{C1})$$

The first step in the calculation of the pair propagator (9) is the evaluation of the frequency integral. Since we only consider the limit of a vanishing impurity density, the fermionic propagator's pole in imaginary frequency representation are in the lower half plane. The frequency integration contour can thus be closed in the upper half plane so that only one of the two poles of the boson propagator  $G_{11}^\phi$  contributes. After analytic continuation, the expression for the pair propagator reduces to (in our new units)

$$L(\Omega, \mathbf{p}) = - \int \frac{d^3k}{(2\pi)^3} \left\{ \frac{\sqrt{k^2(k^2+4)} + k^2 + 2}{2\sqrt{k^2(k^2+4)}} \times \frac{1}{\Omega - \frac{1}{2}\sqrt{k^2(k^2+4)} - \frac{(p-k)^2}{2\alpha} + i0^+} + \frac{2\alpha}{(\alpha+1)k^2} \right\}. \quad (\text{C2})$$

In a second step, we separate  $L$  into its real and imaginary part using the identity  $(x + i0^+)^{-1} = \mathcal{P}(1/x) - i\pi\delta(x)$ , where  $\mathcal{P}$  denotes the principal value. We carry out the angular part of the integration which yields

$$\text{Re}L(\Omega, \mathbf{p}) = - \frac{1}{(2\pi)^2} \int_0^\infty dk \left\{ \alpha \frac{f(k)}{p} \log \left| \frac{g(\Omega, k, p)}{g(\Omega, k, -p)} \right| + \frac{4\alpha}{\alpha+1} \right\}, \quad (\text{C3})$$

where  $f$  denotes the principal value integral, and

$$\text{Im}L(\Omega, \mathbf{p}) = \frac{\alpha}{4\pi} \int_0^\infty dk \frac{f(k)}{p} \{ \theta [g(\Omega, k, p)] - \theta [g(\Omega, k, -p)] \} \quad (\text{C4})$$

with functions  $f$  and  $g$  defined by

$$f(k) = k \frac{\sqrt{k^2(k^2+4)} + k^2 + 2}{2\sqrt{k^2(k^2+4)}} \quad (\text{C5})$$

and

$$g(\Omega, k, p) = \Omega - \frac{1}{2}\sqrt{k^2(k^2+4)} - \frac{(p-k)^2}{2\alpha}. \quad (\text{C6})$$

#### 1. Real part of the pair propagator

Using the substitution  $k = x - 1/x$ , Eq. (C3) becomes

$$\text{Re}L(\Omega, \mathbf{p}) = - \frac{1}{(2\pi)^2} \left\{ \frac{4\alpha}{\alpha+1} + \int_1^\infty dx \left[ \frac{\alpha x}{p} \log \left| \frac{h(\Omega, p, x)}{h(\Omega, -p, x)} \right| + \frac{4\alpha}{\alpha+1} \right] \right\}, \quad (\text{C7})$$

where

$$h(\Omega, p, x) = x^4 - \frac{2p}{\alpha+1}x^3 - \frac{2\alpha}{\alpha+1} \left( \Omega - \frac{p^2}{2\alpha} + \frac{1}{\alpha} \right) + \frac{2p}{\alpha+1}x - \frac{\alpha-1}{\alpha+1} \quad (\text{C8})$$

is a fourth-order polynomial in  $x$ . It can easily be verified from the expression for the function  $h$  that its zeros  $x_i$ ,  $i = 1, \dots, 4$  (which may be calculated analytically) obey the simple identity  $\sum_i x_i = 2p/(\alpha+1)$ . Due to the symmetry  $h(\Omega, -p, x) = h(\Omega, p, -x)$ , the zeros in the denominator in Eq. (C7) are obtained by multiplying  $x_i$  by  $-1$ .

In order to progress further, we rewrite  $h$  as  $h(\Omega, p, x) = \prod_i (x - x_i)$  and decompose the logarithm into a sum of eight logarithms containing one factor each. The integrals to be solved are then of the form  $\int_1^{x_{\max}} dx x \log |x - x_i|$  which is analytically tractable [97]. Writing  $x_j = a_j + ib_j$  with  $a_j, b_j \in \mathbb{R}$ , carrying out the integral, rearranging the sum using the identity  $\sum_i x_i = 2p/(\alpha+1)$  and taking the limit  $x_{\max} \rightarrow \infty$ , one finally obtains the analytical result

$$\text{Re}L(\Omega, \mathbf{p}) = - \frac{1}{(2\pi)^2} \left\{ \frac{2\alpha}{\alpha+1} + \frac{\alpha}{p} \sum_{j=1}^4 [a_j |b_j| \times \left( \pi - \arctan \frac{1+a_j}{|b_j|} - \arctan \frac{1-a_j}{|b_j|} \right) + \frac{1-a_j^2 + b_j^2}{2} \text{atanh} \frac{2a_j}{1+a_j^2 + b_j^2} \right] \right\}. \quad (\text{C9})$$

A considerable simplification occurs for  $\alpha = 1$ . Then the constant term in  $h$  vanishes identically such that in the ratio  $h(x)/h(-x)$  one power of  $x$  cancels, leaving us with the third-order polynomial

$$h(\Omega, p, x) = x^3 - px^2 - \left( \Omega - \frac{p^2}{2} + 1 \right) x + p \quad (\text{C10})$$



with three complex zeros. The result becomes even simpler for the case of  $p = 0$  where  $h$  takes the form of a quadratic polynomial. Carrying out the calculation, one then finds the compact result

$$\operatorname{Re}L(\Omega) = \frac{-1}{2\pi^2} \begin{cases} 1 - \frac{\arctan \sqrt{-1-\Omega}}{\sqrt{-1-\Omega}} \Omega & \Omega < -1 \\ 1 - \frac{\operatorname{atanh} \sqrt{1+\Omega}}{\sqrt{1+\Omega}} \Omega & -1 \leq \Omega \leq 0 \\ 1 - \frac{\operatorname{atanh} \frac{1}{\sqrt{1+\Omega}}}{\sqrt{1+\Omega}} \Omega & 0 < \Omega \end{cases} \quad (\text{C11})$$

which we already quoted in a different set of units in Eq. (11).

## 2. Imaginary part of the pair propagator

The calculation of the imaginary part of the pair propagator is considerably simpler. Since the Heaviside functions inside the integrand in Eq. (C4) do nothing but change the limits of integration, one is left with an integral over  $f(k)$  yielding

$$\operatorname{Im}L(\Omega, \mathbf{p}) = \frac{\alpha}{16\pi p} \left( k^2 + \sqrt{k^2(k^2 + 4)} \right) \Big|_{k_{\min}(\Omega, \mathbf{p})}^{k_{\max}(\Omega, \mathbf{p})}, \quad (\text{C12})$$

where  $k_{\min}$  and  $k_{\max}$  denote the real and positive zeros of the functions  $g(\Omega, k, p)$  and  $g(\Omega, k, -p)$  defined by Eq. (C6).

Studying the properties of the function  $g$ , one finds the very simple result that for small external momenta

the onset for a nonzero  $\operatorname{Im}L$  as function of frequency for given momentum  $p$  obeys the exact relation

$$\Omega_{\min}(p) = -g(0, 0, p) = \frac{p^2}{2\alpha} \quad (p \leq \alpha), \quad (\text{C13})$$

which can be viewed as a consequence of the Landau criterion for the onset of superfluidity.

As in the case of the real part, it is insightful to consider the limiting case  $p = 0$ . In this limit,  $k_{\min}$  and  $k_{\max}$  converge towards the same value and the expression in Eq. (C4) becomes a derivative with respect to  $p$ . Calculating the derivative and then carrying out the integral one finds

$$\operatorname{Im}L(\Omega, 0) = \frac{k_0}{4\pi} \frac{\sqrt{k_0^2(k_0^2 + 4)} + k_0^2 + 2}{\alpha^{-1} \sqrt{k_0^2(k_0^2 + 4)} + k_0^2 + 2}, \quad (\text{C14})$$

where  $k_0 = k_0(\Omega)$  is the solution to the equation  $g(\Omega, k_0, 0) = 0$  which is readily calculated analytically. Again, the expression becomes particularly simple in the case  $\alpha = 1$  where one finds [cf. Eq. (12)]

$$\operatorname{Im}L(\Omega, 0) = \frac{1}{4\pi} \frac{\Omega}{\sqrt{1+\Omega}} \theta(\Omega). \quad (\text{C15})$$

To illustrate the results of this Appendix, we show the real and imaginary part of the pair propagator for the mass-balanced case  $\alpha = 1$  in Fig. 10.

- 
- [1] P. W. Anderson, Phys. Rev. Lett. **18**, 1049 (1967).
  - [2] L. D. Landau, Phys. Z. Sowjetunion **3**, 644 (1933).
  - [3] L. D. Landau and S. I. Pekar, J. Exp. Theor. Phys. **18**, 419 (1948).
  - [4] H. Fröhlich, Adv. Phys. **3**, 325 (1954).
  - [5] M. Girardeau, Phys. Fluid. **4**, 279 (1961).
  - [6] I. Bloch, J. Dalibard, and W. Zwerger, Rev. Mod. Phys. **80**, 885 (2008).
  - [7] M. Koschorreck, D. Pertot, E. Vogt, B. Fröhlich, M. Feld, and M. Köhl, Nature **485**, 619 (2012).
  - [8] R. Schmidt and T. Enss, Phys. Rev. A **83**, 063620 (2011).
  - [9] C. Kohstall, M. Zaccanti, M. Jag, A. Trenkwalder, P. Massignan, G. M. Bruun, F. Schreck, and R. Grimm, Nature **485**, 615 (2012).
  - [10] A. P. Chikkatur, A. Görlitz, D. M. Stamper-Kurn, S. Inouye, S. Gupta, and W. Ketterle, Phys. Rev. Lett. **85**, 483 (2000).
  - [11] J. Catani, G. Lamporesi, D. Naik, M. Gring, M. Inguscio, F. Minardi, A. Kantian, and T. Giamarchi, Phys. Rev. A **85**, 023623 (2012).
  - [12] N. Spethmann, F. Kindermann, S. John, C. Weber, D. Meschede, and A. Widera, Phys. Rev. Lett. **109**, 235301 (2012).
  - [13] R. Scelle, T. Rentrop, A. Trautmann, T. Schuster, and M. K. Oberthaler, arXiv 1306.3308 (2013).
  - [14] C. Ospelkaus, S. Ospelkaus, L. Humbert, P. Ernst, K. Sengstock, and K. Bongs, Phys. Rev. Lett. **97**, 120402 (2006).
  - [15] C.-H. Wu, I. Santiago, J. W. Park, P. Ahmadi, and M. W. Zwierlein, Phys. Rev. A **84**, 011601 (2011).
  - [16] J. W. Park, C.-H. Wu, I. Santiago, T. G. Tiecke, S. Will, P. Ahmadi, and M. W. Zwierlein, Phys. Rev. A **85**, 051602 (2012).
  - [17] C.-H. Wu, J. W. Park, P. Ahmadi, S. Will, and M. W. Zwierlein, Phys. Rev. Lett. **109**, 085301 (2012).
  - [18] G. E. Astrakharchik and L. P. Pitaevskii, Phys. Rev. A **70**, 013608 (2004).
  - [19] F. M. Cucchiatti and E. Timmermans, Phys. Rev. Lett. **96**, 210401 (2006).
  - [20] K. Sacha and E. Timmermans, Phys. Rev. A **73**, 063604 (2006).
  - [21] R. M. Kalas and D. Blume, Phys. Rev. A **73**, 043608 (2006).
  - [22] M. Bruderer, W. Bao, and D. Jaksch, Eur. Phys. Lett. **82**, 30004 (2008).
  - [23] A. A. Blinova, M. G. Boshier, and E. Timmermans, arXiv 1304.7704 (2013).
  - [24] J. Tempere, W. Casteels, M. K. Oberthaler, S. Knoop, E. Timmermans, and J. T. Devreese, Phys. Rev. B **80**, 184504 (2009).

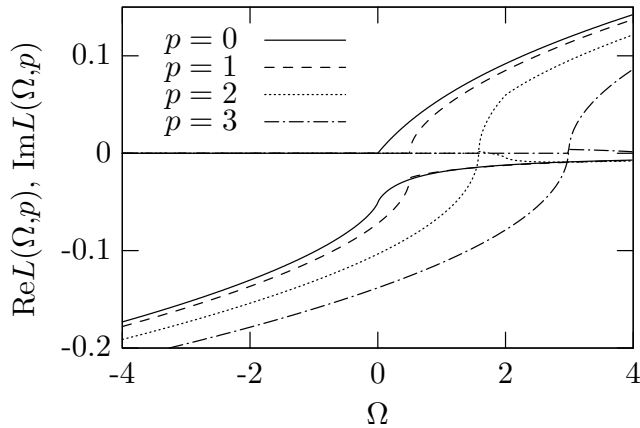


FIG. 10: Real and imaginary part of the pair propagator  $L$  for  $\alpha = 1$  and different values of the external momentum  $p$ .  $\text{Im}L$  is strictly positive while  $\text{Re}L$  is mostly negative. Note that this figure uses units in which  $g_{\phi\phi}\rho_0 = 1$ .

- [25] W. Casteels, J. Tempere, and J. T. Devreese, Phys. Rev. A **83**, 033631 (2011).
- [26] W. Casteels, T. V. Caueren, J. Tempere, and J. T. Devreese, Laser Physics **21**, 1480 (2011).
- [27] W. Casteels, J. Tempere, and J. T. Devreese, Phys. Rev. A **84**, 063612 (2011).
- [28] W. Casteels, J. Tempere, and J. T. Devreese, Phys. Rev. A **86**, 043614 (2012).
- [29] D. Dasenbrook and A. Komnik, Phys. Rev. B **87**, 094301 (2013).
- [30] H. T. C. Stoof, M. Houbiers, C. A. Sackett, and R. G. Hulet, Phys. Rev. Lett. **76**, 10 (1996).
- [31] M. J. Bijlsma, B. A. Heringa, and H. T. C. Stoof, Phys. Rev. A **61**, 053601 (2000).
- [32] H. Heiselberg, C. J. Pethick, H. Smith, and L. Viverit, Phys. Rev. Lett. **85**, 2418 (2000).
- [33] F. Matera, Phys. Rev. A **68**, 043624 (2003).
- [34] D.-W. Wang, Phys. Rev. Lett. **96**, 140404 (2006).
- [35] T. Enss and W. Zwerger, Eur. Phys. J. B **68**, 383 (2009).
- [36] J. T. Stewart, J. P. Gaebler, and D. S. Jin, Nature **454**, 744 (2008).
- [37] A. Schirotzek, C.-H. Wu, A. Sommer, and M. W. Zwierlein, Phys. Rev. Lett. **102**, 230402 (2009).
- [38] M. Feld, B. Fröhlich, E. Vogt, M. Koschorreck, and M. Köhl, Nature **480**, 75 (2011).
- [39] C. Chin, R. Grimm, P. Julienne, and E. Tiesinga, Rev. Mod. Phys. **82**, 1225 (2010).
- [40] N. M. Hugenholtz and D. Pines, Phys. Rev. **116**, 489 (1959).
- [41] A. A. Abrikosov, L. P. Gorkov, and I. E. Dzialoshinski, *Methods of Quantum Field Theory in Statistical Physics* (Dover, New York, 1975).
- [42] C. G. Kuper, Phys. Rev. **122**, 1007 (1961).
- [43] A. Sartori and A. Recati, arXiv 1305.2094 (2013).
- [44] S. T. Belyaev, Sov. Phys. JETP **7**, 289 (1958).
- [45] H. Shi and A. Griffin, Phys. Rep. **304**, 1 (1998).
- [46] B. Capogrosso-Sansone, S. G. Söyler, N. Prokof'ev, and B. Svistunov, Phys. Rev. A **77**, 015602 (2008).
- [47] M. Punk and W. Zwerger, Phys. Rev. Lett. **99**, 170404 (2007).
- [48] R. Combescot, A. Recati, C. Lobo, and F. Chevy, Phys. Rev. Lett. **98**, 180402 (2007).
- [49] A. Perali, P. Pieri, and G. C. Strinati, Phys. Rev. Lett. **100**, 010402 (2008).
- [50] P. Massignan, G. M. Bruun, and H. T. C. Stoof, Phys. Rev. A **77**, 031601 (2008).
- [51] T. Enss, Phys. Rev. A **86**, 013616 (2012).
- [52] P. Nozières and S. Schmitt-Rink, J. Low Temp. Phys. **59**, 195 (1985).
- [53] F. Chevy, Phys. Rev. A **74**, 063628 (2006).
- [54] N. Prokof'ev and B. Svistunov, Phys. Rev. B **77**, 020408 (2008).
- [55] N. V. Prokof'ev and B. V. Svistunov, Phys. Rev. B **77**, 125101 (2008).
- [56] E. Fratini and P. Pieri, Phys. Rev. A **81**, 051605 (2010).
- [57] T. Weber, J. Herbig, M. Mark, H.-C. Nägerl, and R. Grimm, Science **299**, 232 (2003).
- [58] T. Kraemer, M. Mark, P. Waldburger, J. G. Danzl, C. Chin, B. Engeser, A. D. Lange, K. Pilch, A. Jaakkola, H.-C. Nägerl, and R. Grimm, Nature **440**, 315 (2006).
- [59] N. Navon, S. Piatecki, K. Günter, B. Rem, T. C. Nguyen, F. Chevy, W. Krauth, and C. Salomon, Phys. Rev. Lett. **107**, 135301 (2011).
- [60] P. Makotyn, C. E. Klaus, D. L. Goldberger, E. A. Cornell, D. S. Jin, arXiv 1308.3696 (2013).
- [61] G.-B. Jo, Y.-R. Lee, J.-H. Choi, C. A. Christensen, T. H. Kim, J. H. Thywissen, D. E. Pritchard, and W. Ketterle, Science **325**, 1521 (2009).
- [62] M. Barth and W. Zwerger, Annals of Physics **326**, 2544 (2011).
- [63] V. B. Shenoy and T.-L. Ho, Phys. Rev. Lett. **107**, 210401 (2011).
- [64] X. Cui and H. Zhai, Phys. Rev. A **81**, 041602 (2010).
- [65] P. Massignan and G. Bruun, Eur. Phys. J. D **65**, 83 (2011).
- [66] M. Punk, P. T. Dumitrescu, and W. Zwerger, Phys. Rev. A **80**, 053605 (2009).
- [67] C. Mora and Y. Castin, Phys. Rev. Lett. **102**, 180404 (2009).
- [68] F. M. Marchetti, C. J. M. Mathy, D. A. Huse, and M. M. Parish, Phys. Rev. B **78**, 134517 (2008).
- [69] Z.-Q. Yu, S. Zhang, and H. Zhai, Phys. Rev. A **83**, 041603 (2011).
- [70] E. Fratini and P. Pieri, Phys. Rev. A **85**, 063618 (2012).
- [71] R. Haussmann, W. Rantner, S. Cerrito, and W. Zwerger, Phys. Rev. A **75**, 023610 (2007).
- [72] R. Haussmann, M. Punk, and W. Zwerger, Phys. Rev. A **80**, 063612 (2009).
- [73] T. Enss, R. Haussmann, and W. Zwerger, Annals of Physics **326**, 770 (2011).
- [74] T. Enss and R. Haussmann, Phys. Rev. Lett. **109**, 195303 (2012).
- [75] M. J. H. Ku, A. T. Sommer, L. W. Cheuk, and M. W. Zwierlein, Science **335**, 563 (2012).
- [76] K. Van Houcke, F. Werner, E. Kozik, N. Prokof'ev, B. Svistunov, M. J. H. Ku, A. Sommer, L. W. Cheuk, A. Schirotzek, and M. W. Zwierlein, Nature Physics **8**, 366 (2012).
- [77] T.-L. Dao, A. Georges, J. Dalibard, C. Salomon, and I. Carusotto, Phys. Rev. Lett. **98**, 240402 (2007).
- [78] V. N. Efimov, Phys. Lett. B **33**, 563 (1970).
- [79] K. Helfrich, H.-W. Hammer, and D. S. Petrov, Phys. Rev. A **81**, 042715 (2010).
- [80] N. T. Zinner, Europhys. Lett. **101**, 60009 (2013).
- [81] K. Góral, T. Köhler, S. A. Gardiner, E. Tiesinga, and

- P. S. Julienne, J. Phys. B **37**, 3457 (2004).
- [82] M. H. Szymańska, K. Góral, T. Köhler, and K. Burnett, Phys. Rev. A **72**, 013610 (2005).
- [83] F. Werner, L. Tarruell, and Y. Castin, Eur. Phys. J. B **68**, 401 (2009).
- [84] R. Combescot, S. Giraud, and X. Leyronas, Eur. Phys. Lett. **88**, 60007 (2009).
- [85] P. Massignan, Eur. Phys. Lett. **98**, 10012 (2012).
- [86] R. Schmidt, Ph.D. thesis, Technische Universität München (2013).
- [87] S. Zöllner, G. M. Bruun, and C. J. Pethick, Phys. Rev. A **83**, 021603 (2011).
- [88] R. Schmidt, T. Enss, V. Pietilä, and E. Demler, Phys. Rev. A **85**, 021602 (2012).
- [89] T. Watanabe, T. Suzuki, and P. Schuck, Phys. Rev. A **78**, 033601 (2008).
- [90] T. Sogo, P. Schuck, and M. Urban, arXiv 1307.1147 (2013).
- [91] L. D. Landau and E. M. Lifshitz, in *Quantum mechanics* (Butterworth-Heinemann, 1987), vol. III of *Course of Theoretical Physics*.
- [92] Note that the presence of a *finite* density of fermions can induce a collapse or phase separation of the BEC beyond a critical interaction strength. This instability is due to fermionic particle–hole fluctuations giving rise to a Lindhard type softening of the Bogoliubov modes [34, 35]. In our case,  $n_\psi \rightarrow 0$ , and such an effect, which is different from the self-localization aspect to be discussed below, does not take place.
- [93] In contrast to the Fermi polaron where the host medium is given by a non-interacting Fermi sea with low compressibility due to Fermi pressure, such a response of a BEC to the presence of a single impurity may be significant since here the host medium is a highly compressible fluid.
- [94] This results in a set of four different T-matrices which differ in the kind of incoming and outgoing bosonic particle (condensate or non-condensate). Two of these T-matrices appear for instance in the impurity self-energy [cf. Fig. 1 (b)]. It turns out that within both the self-consistent and the non-selfconsistent T-matrix approximation all four vertices are represented by the same (amputated) vertex  $\Gamma_{\phi\psi}$ .
- [95] In terms of the two-channel model discussed in Appendix A, the second term may be interpreted as an effective boson–molecule repulsion.
- [96] We have also compared some of the data discussed here to results obtained in a hybrid selfconsistent approximation where one uses the T-matrix and boson propagator for an interacting condensate, but neglects the one-loop correction to the selfenergy. We find that the differences between a finite and a vanishing  $g_{\phi\phi}$  are even smaller in the selfconsistent approximation.
- [97] Note the introduction of a finite upper limit  $x_{\max}$ . Although the overall integrand is convergent, the terms in the sum are not convergent individually. After integrating and summing up, the limit  $x_{\max} \rightarrow \infty$  may safely be taken.